T-61990

07821-6004-R0-00

RESEARCH PROGRAM ON HOLOGRAPHIC INSTRUMENTATION

Final Report

June 15, 1968

Prepared by L. O. Heflinger

R. E. Brooks

Approved by A. V. Haeff

Prepared Under

Contract NASW-1572

For

National Aeronautics and Space Administration
Headquarters
Washington, D. C. 20546

By

TRW Systems
One Space Park, Redondo Beach, California 90278

TABLE OF CONTENTS

TABLE OF CONTENTS (Cont'd)

ABSTRACT

This report describes investigations conducted to improve instrumentation techniques by the application of holography. Methods for producing holograms suited to particle impact studies and several holographic interferometer systems are described. Some interferometer techniques useful in obtaining increased sensitivity are analyzed and experimentally tested.

1.0 INTRODUCTION AND SURVEY

The objective of this program on holographic instrumentation, funded through NASA headquarters and monitored through NASA Ames, has been to develop improved holographic instrumentation techniques applicable to NASA programs. Particular emphasis was placed during this program on an attempt to improve the sensitivity of optical aerodynamic flow monitoring techniques, that is shadowgraph, schlieren, and interferometry techniques.

The need for improved sensitivity arises from the simulation requirements of re-entering capsules. For proper simulation, the air density must be low, which renders its effect on light waves very small. In this program to improve flow instrumentation by holographic techniques, bullets have been used to test out the techniques since they constitute a very inexpensive readily available source of shock waves with known and controllable properties. When used in conjunction with a small vacuum chamber, they permit simulation of the shocks of re-entering capsules, adequate for testing of the holographic techniques.

A number of different investigations were conducted during the program to evaluate various possible approaches to improved instrumentation. These investigations are described in the remainder of this report.

Section 2 describes improvements made to the basic pulsed laser holographic setup, which was on hand at the outset of the program. The improved quality of the holographic images are illustrated by photos of high speed fragments as might be encountered in cratering studies, and by interferograms of shock layers.

Section 3 describes an extension to front-lighted subjects of the path matching techniques used in the basic rear illumination technique of Section 2. The path matching principles have permitted pulsed holography of small front-lighted scenes with lasers of limited coherence.

Section 4 describes experiments in which a low density chamber was used in the basic holocamera. This chamber allowed interferograms to be made of shocks at the sensitivity limit of interferometry.

Section 5 describes attempts to improve the sensitivity limit by making interferograms in which a constant phase shift throughout the scene is introduced, so as to maximize the intensity variations from small subject phase shifts. Experimental difficulties with pulsed laser tests, where shocks permit quantitative evaluation of the sensitivity, have prevented a thorough evaluation of this approach. It appears likely that some gain over regular infinite fringe interferograms can be achieved, but its value in comparison with conventional fringe interpolation techniques has not been determined yet.

Section 6 and its related appendix describe a system developed to place a grid of finite fringes in a specified plane of the hologram's virtual image space. This permits the subject and finite fringe grid to appear in focus at the same location. This technique extends the usefulness of the finite fringe method to holographic interferometry, and may permit the production of extremely accurate finite fringe background grids since the accuracy is not dependent on optical quality, but only on the ability to perform a rigid rotation.

Section 7 describes an experiment in which pulsed holographic interferograms were made with ultraviolet light obtained from doubled ruby light. This technique gains a factor of two in sensitivity over direct use of the ruby laser.

Section 8 describes a new method developed in this program for producing interferograms with increased sensitivity. The improvement in sensitivity stems from the use of high orders of diffraction, and the holographic system utilized preserves the insensitivity to optical quality and precision alignment characteristic of holographic systems. The method has been demonstrated to give a factor of four increase in the number of fringes, and further improvement in sensitivity is believed possible.

Section 9 describes analysis and experiments done in order to determine the extent that holographic techniques make practical multiple pass interferometers with their increased sensitivity. Experimental results with a 10-pass system show encouraging results.

The reader may note that several of the systems for obtaining improved sensitivity are theoretically compatible with each other.

Section 10 illustrates a simple beginning towards a combination of systems. The apparatus is basically an arrangement similar to the Michelson configuration which permits double pass interferograms to be made of shock phenomena. The arrangement will be tested with the high order interferometry method. As of the time of writing, the system has been tested with regular first order holographic interferometry using a Q-switched ruby laser, and demonstrates the ease with which holographic interferograms can be made without precision optics or alignment.

2.0 IMPROVEMENT OF QUALITY OF HOLOGRAMS

The basic arrangement used for the production of holograms with the pulsed laser is shown in Fig. 2-1, which is reproduced from reference 1. This arrangement was designed to produce 4" x 5" holograms which allow the object to be viewed over about a 40 degree angular range. The scene volume is approximately 4 x 4 x 4 inches with the restriction that the reference beam passes through a portion of this volume, restricting the useful volume by one-half for some applications.

To understand the operation of this holocamera, consider a single ray from the laser source. This ray is first split into a reference and scene ray, and then the scene ray is in turn split into many rays by the ground glass. The fundamental design principle is that all of these rays, derived from the same parent ray, arrive at the hologram at essentially the same point and with essentially the same optical delay. The configuration shown in Fig. 2-1 achieves these conditions for each ray from the laser. Thus only local transverse coherence is required of the laser, and the temporal coherence required is set only by the residual errors in the path length matching process*

---

* For convenience, we reproduce here from reference 1 the description of the functioning of the various components of the "focused ground glass" arrangement. Fig. 2-1 shows "a configuration which permits a diffusing screen to be employed with large diffusing angles without destroying the spatial match. In this arrangement, the diffuser is focused onto the hologram with a pair of plano convex lenses bringing the diffuse rays back into correct correspondence with the rays of the reference beam. A second pair of lenses, identical to the pair used for focusing the diffuser, is inserted next to the diffuser and directs the diffuse light toward the focusing lenses; at the same time, they also compensate for the increasing path lengths at increasing distances from the diffuser's center. Because the reference beam arrives at the hologram at an angle β to the plate, the path lengths are longer on one side than on the other. Similar path length differences are produced in the scene beam by directing it onto the diffuser at the same angle β. An array of small prisms is used behind the diffuser to direct the scene beam toward the hologram, making optimum use of the light.

"This arrangement permits spatial and temporal matching of the reference beam with the diffuse scene light to within the limits set by the aberrations of the lenses. It has been tested with the subject placed approximately midway between the hologram and the focusing lenses. With this arrangement, it is possible to view the recorded scene over about 40° with reasonably uniform diffuse illumination."

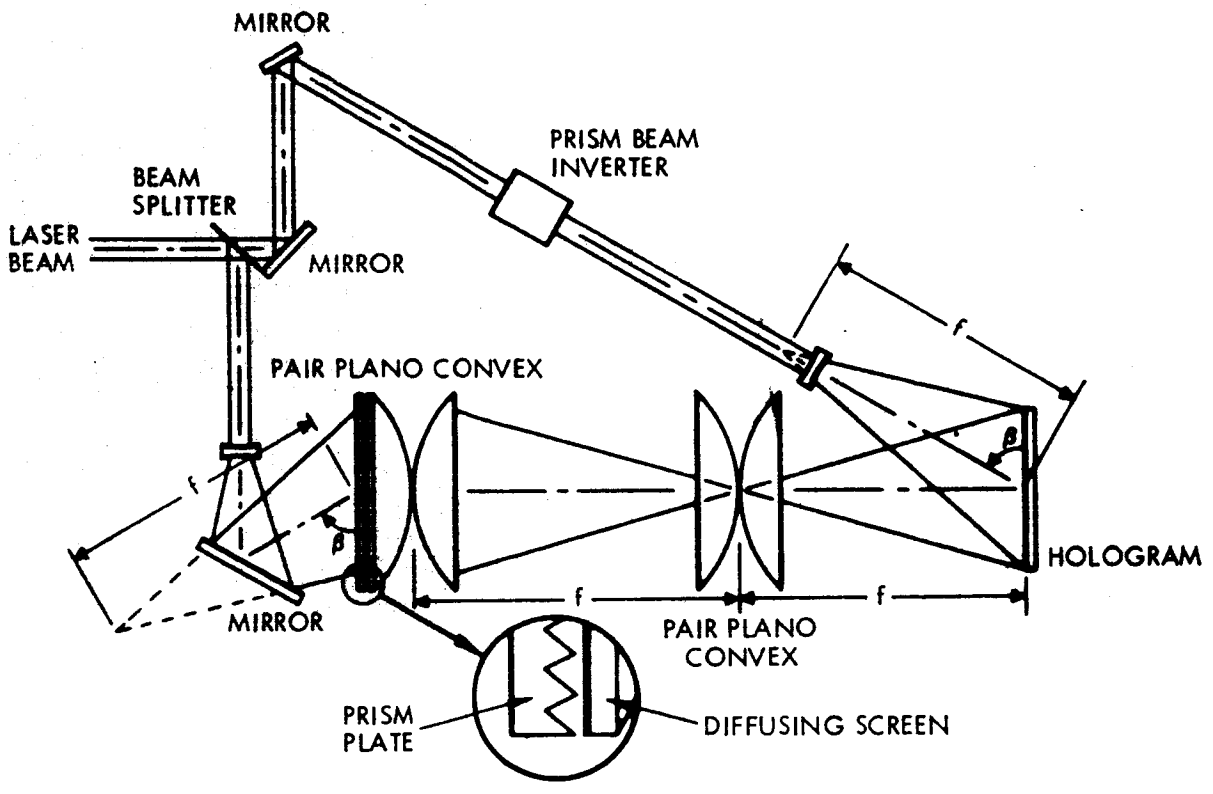

Fig. 2-1. Two-Beam holographic arrangement using a focused diffuser to provide spatial matching.

The improvements made in the picture quality during this program all stem from small improvements, which taken together, however, have produced a very marked improvement in the quality of the reconstructed images. These individually small improvements are:

1. Painting the back side of the hologram plates, before exposure, with flat black spray paint. This removes the reflection from this rear surface and produces holograms of greater scene intensity and with less scattered light, giving higher contrast. The black paint can be scraped off the glass plate fairly easily after development while the plate is wet. We have not yet tried the standard, antihalation coating offered by the manufacturer. The plates used were Kodak type 649F.

2. Better uniformity of lighting of the background glass diffuser has been obtained by using a second ground glass at a distance of about one inch from the first. While this slightly spoils the transverse matching of the holocamera, the laser coherence is capable of tolerating the mismatch.

3. The coherence of the laser has been improved by the utilization of a new high quality ruby in the oscillator cavity and by aperturing off all but a selected portion of this ruby.

4. Better path length matching in the holocamera has been achieved, giving holograms of improved brightness and contrast. Traveling wave oscilloscope monitoring of the output pulse shape has shown that the oscillator is self mode locking which gives a temporal coherence function of very complex shape. This is perhaps related to why a few millimeters of path length change can influence the hologram quality even though holograms can be obtained with several centimeters of path length mismatch.

5. Improved alignment of the two amplifier rubies has prevented reflections occurring at the amplifier's faces from entering the holocamera. Better uniformity of exposure of the hologram has resulted, giving in turn an improvement in the ability of the hologram to function over almost all of the 4" x 5" plate.

While it is not possible to preserve all the features of three dimensional holographic images by the conventional photographs reproduced in this report, perhaps the copies shown on the following pages will convey some idea of what can be accomplished by the holographic technique. Six of the holograms from which some of the following pictures were made were delivered to the contract monitor, Ben Beam, NASA Ames.

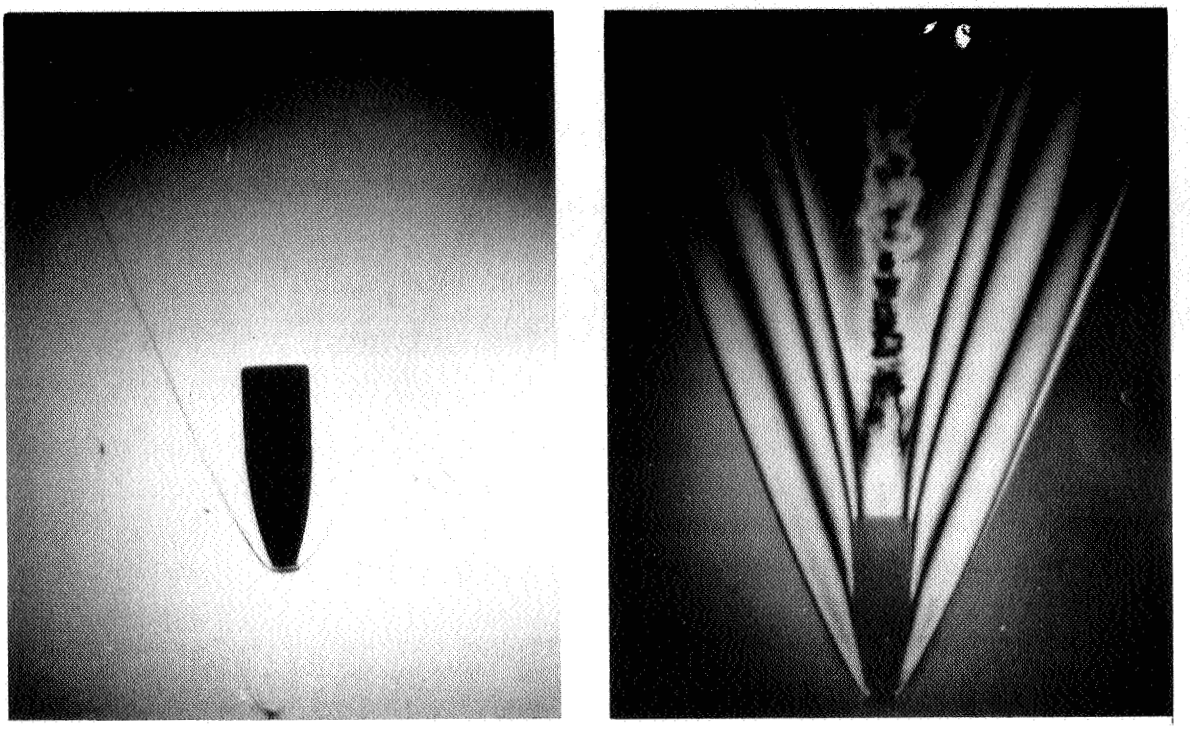

Fig. 2-2. Left: Copy from a single exposure hologram of 22-250 bullet in flight in air at atmospheric pressure. Small fragments are from 1 mil shim stock. Right: Copy from a double exposure interferogram of same type of bullet.

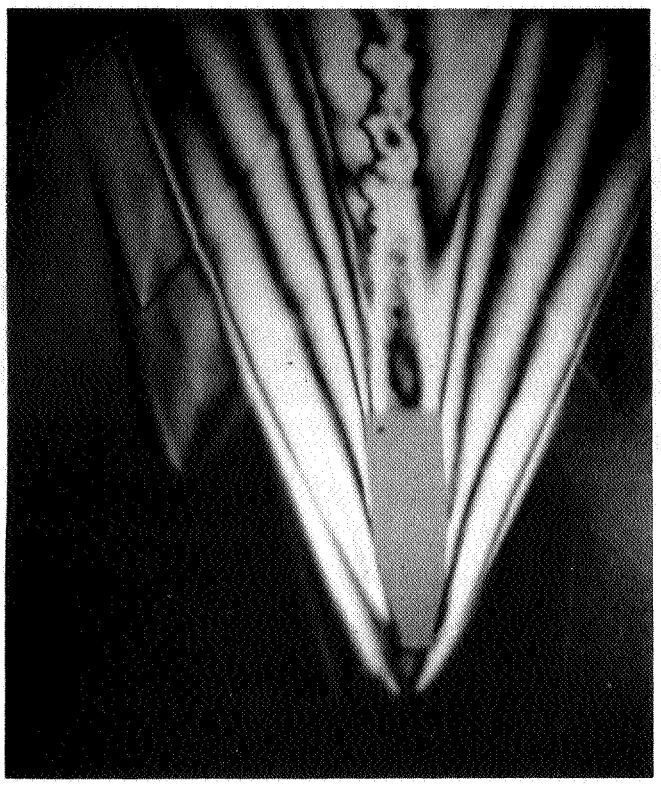

Fig. 2-3. Double exposure interferogram of a bullet which has just passed through .04 mm brass shim stock. When viewing the original hologram the spatial configuration of the small fragments is readily apparent due to the three-dimensional nature of the reconstruction. Of interest here are the small fractional fringe displacements associated with the small fragments. Note the particle on the left slightly above center which is nearly in focus on this copy. The particle's wake appears as a light streak. Note also the shock from this particle and its extension into the shock layer of the main bullet. Within the shock layer of the bullet the displacement of the main fringes by the small particle shock is only about one-fifth of a fringe.

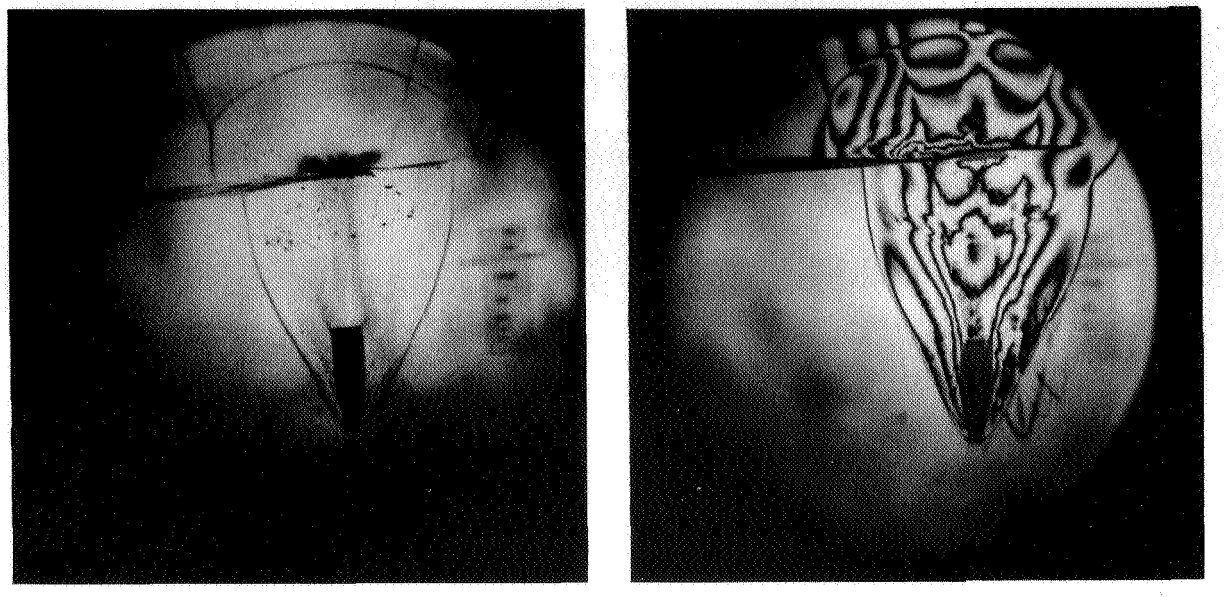

Fig. 2-4. Left: Copy from a single exposure hologram showing bullet passing through .04 mm. brass shim stock. On the original hologram the distribution in space of particles above the plate, just below the plate and near the bullet are evident and can be quantitatively measured. Just above the shim stock is a toroid of unresolvable dark material. A streak of this unresolvable dark material also appears along the path of the bullet between the bullet and shim. Right: A double exposure interferogram of an event nearly identical to the above. On the original hologram it is possible to trace the outline of the shock wave which has passed through the shim stock. It occupies a position almost symmetrical to the reflected shock appearing above the shim stock. The transmitted shock can even be traced into the region outside the bullet shock layer.

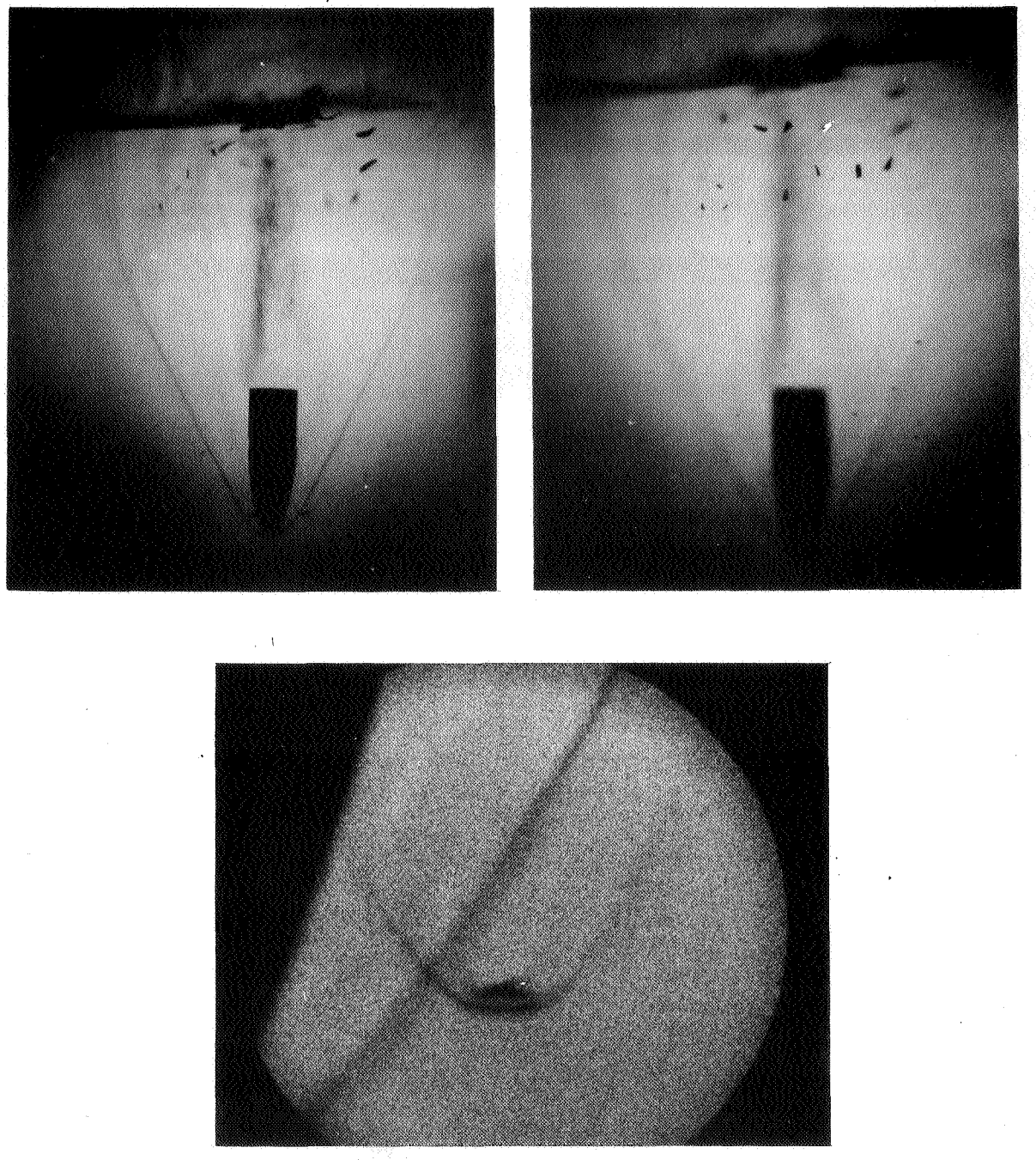

Fig. 2-5. An event similar to that of Fig. 2-4 but shown at greater magnification. All three of these copies are from the same hologram. The copy camera was focused on different focal planes in an attempt to show the wealth of detail available in the original hologram. The lower photo shows a magnified view of a small flat particle traveling broadside. This particle is located just to the right of the bullet. Direct examination of the hologram with a long working distance magnifier gives a better impression of sharpness than is revealed in these copies. To obtain maximum resolution from the holograms it is essential to get the reconstruction point source precisely located relative to the hologram.

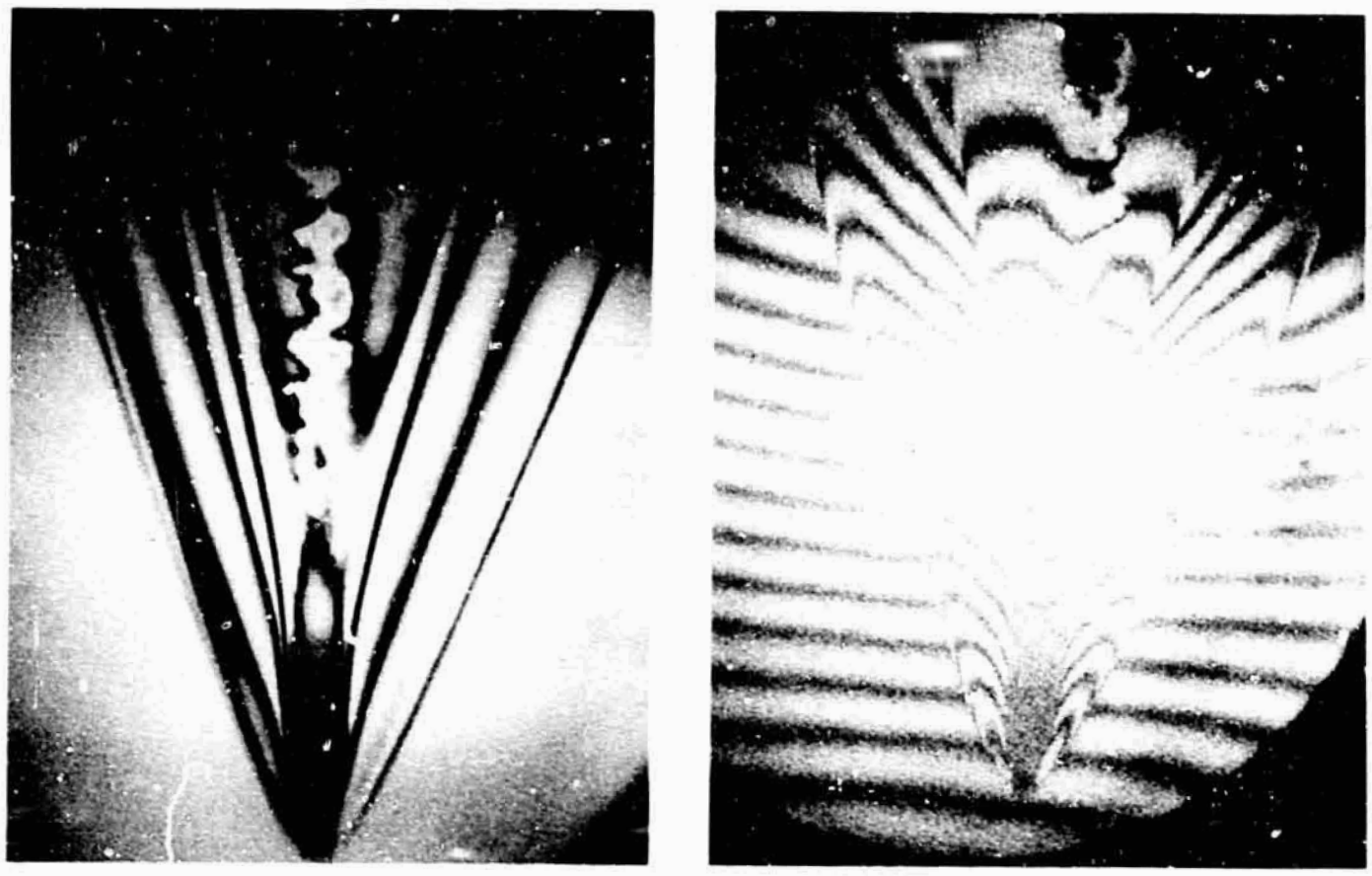

Fig. 2-6. Infinite fringe and finite fringe interferograms of slightly skew bullets in flight. Both are copies from double exposure interferograms. No motion of the apparatus took place between the exposures for the left exposure. For the right picture, a small motion of the hologram plate was made between the exposures, introducing a background of fringes. Because of the lack of precise control of this motion the fringes form in a different plane than the bullet plane. This makes copying difficult. This copy was made at f/16. Copies made at f/2 show no fringes. Visual viewing gives a better impression than does the above copy due to the eye's ability to accommodate and tolerate coarser granularity.

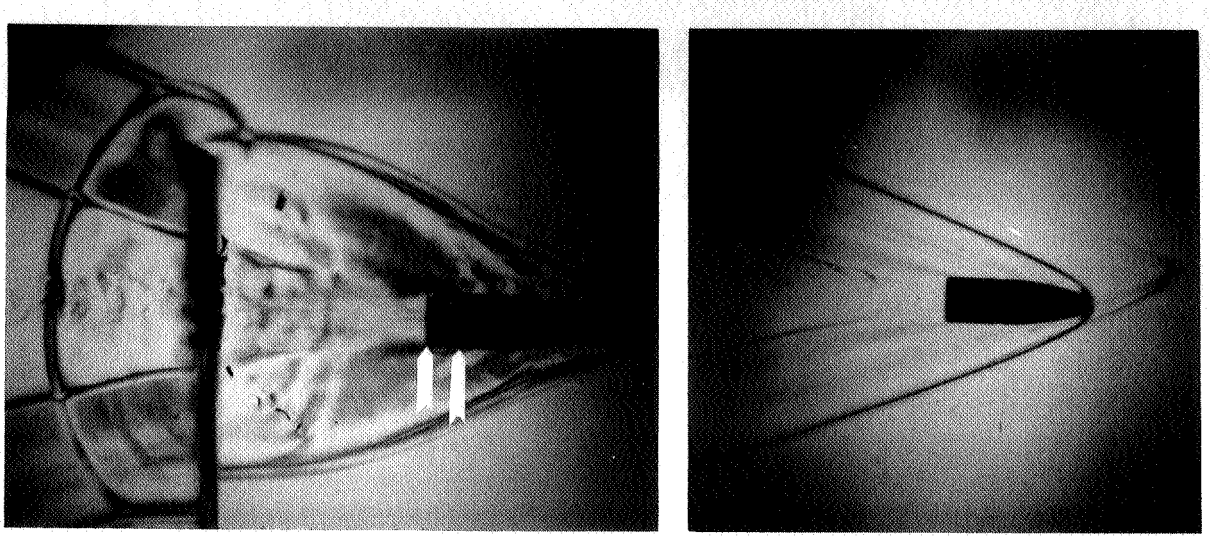

Fig. 2-7. Two examples of differential double exposure holographic interferograms. The left picture was made with two laser pulses separated by approximately three microseconds. The white arrows indicate the amount of bullet motion during this interval. The movement of the shock fronts during this interval are readily seen. Within the shock layer and wake, interference effects are visible which stem from the change in optical path during the time interval. The right picture was made with a laser pulse of about one-half microsecond duration. Here the differential interference makes visible those parts of the pattern which are changing most rapidly. The result has some similarity to a schlieren photograph with a knife edge perpendicular to the bullet path. Both of these photographs resulted from a spontaneous behavior of the laser that is at present not under deliberate control.

3.0 PULSED LASER HOLOGRAMS MADE WITH REFLECTED LIGHT

The basic principle of having each component from the same parent laser ray arrive at the same time and place on the hologram plate has been applied to holograph diffuse objects which can only be illuminated by reflection. The configuration is somewhat similar to Fig. 2-1, but in this case the object occupies the location of the ground glass diffuser and the condenser lenses focus the light reflected from the object onto the hologram plate. Fig. 3-1 shows the arrangement used. The reconstructed image occurs near the hologram plate. The focusing of the condenser lenses is so poor that no trace of a conventional photographic image can be seen on the holograms. However, the focusing is good enough so that in spite of the limited transverse coherence of the laser, interference is achieved and reasonable quality holograms giving three dimensional reconstructions have been made.

The technique makes possible the production of interferograms showing the displacement of a diffuse surface which occurred between the two exposures, as shown in Figures 3-2 and 3-3.

The motion restrictions are more stringent for objects viewed in reflection than are the restrictions for objects illuminated in silhouette. A qualitative test of the motion sensitivity has been made by holographing a rapidly rotating disc, as shown in Figure 3-4.

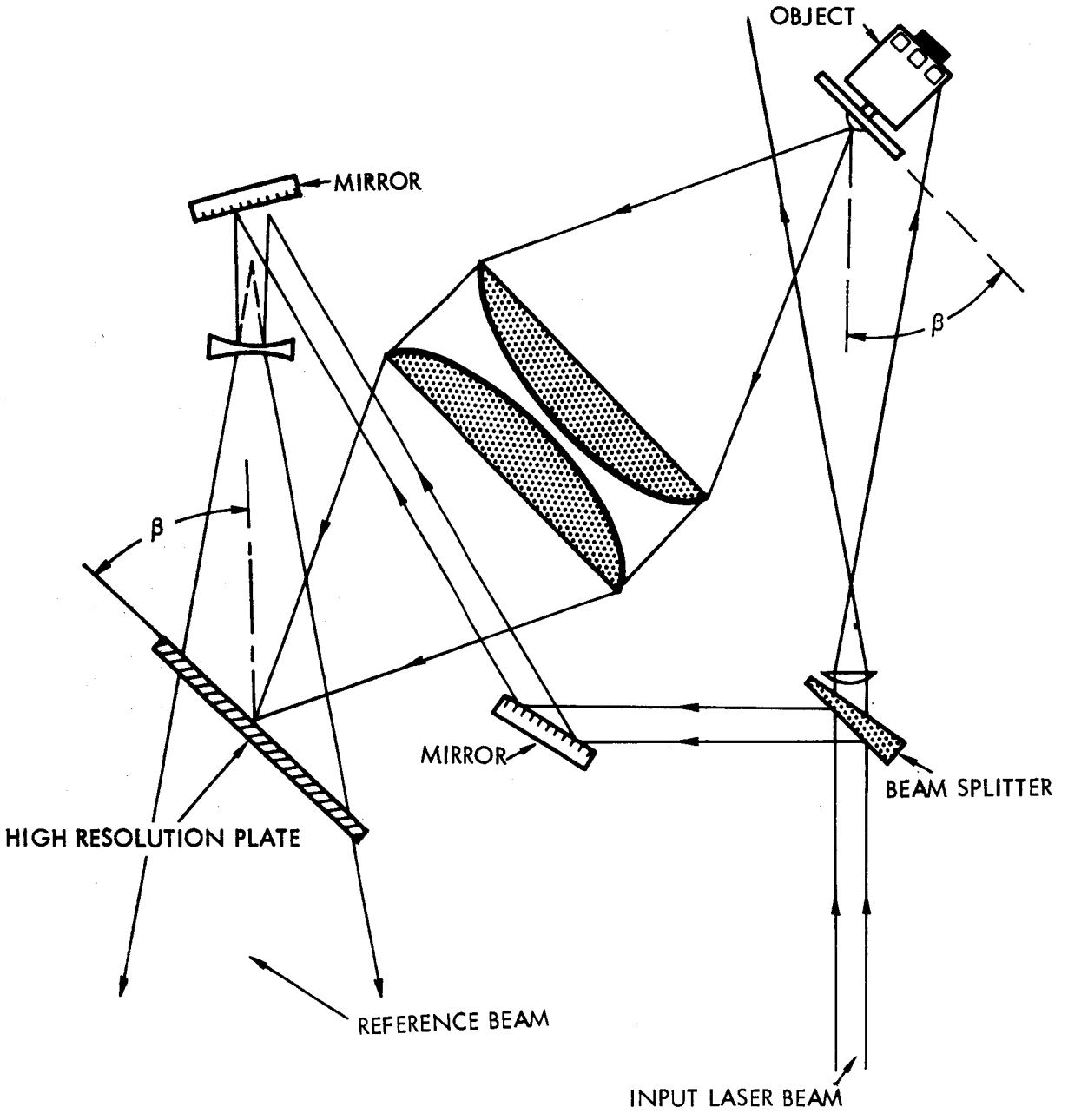

Fig. 3-1. Optical schematic of the holographic arrangement used to make holograms of objects using front illumination with a pulsed ruby laser.

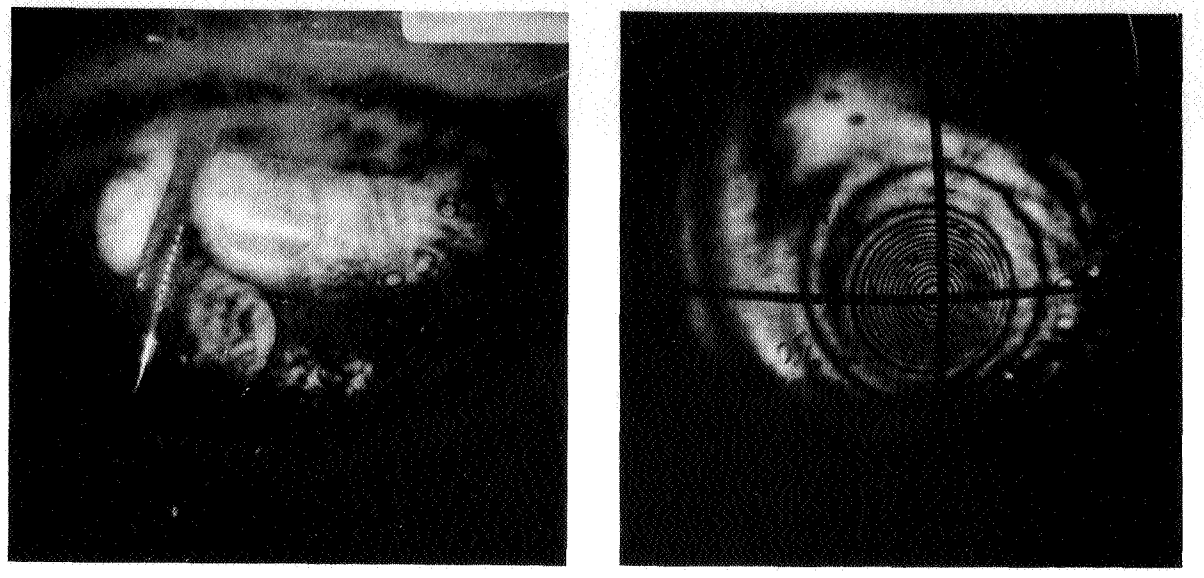

Fig. 3-2. Pulsed laser holograms of objects illuminated by reflected light. Left: A thumb and fingers holding a mechanical pencil. This copy shows the scene size presently possible by reflected light. The depth of scene possible is of the same order as the transverse dimension. The low speed of the 649F emulsion is the primary factor limiting the transverse dimension. Laser coherence limits the longitudinal (depth) dimension. Right: Interferogram showing a contour map of the transient deformation of brass plate which was impacted by a small steel ball 25 microseconds earlier. The brass plate was painted white and the reference lines have tic marks at half centimeter intervals. Plate thickness is 0.6 mm.

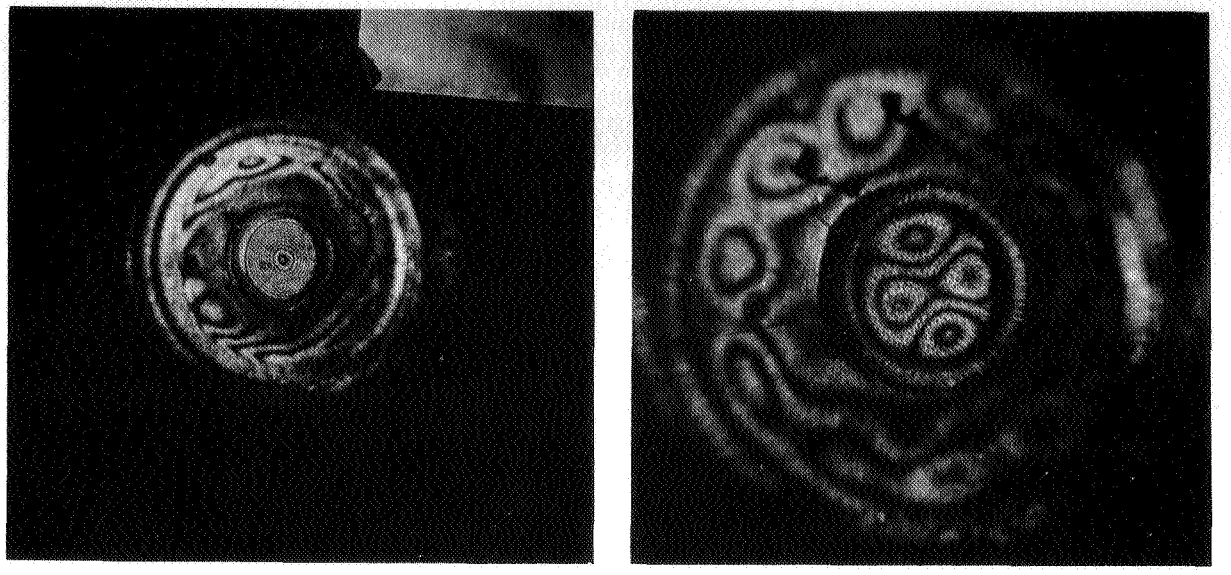

Fig. 3-3. Interferograms of a two-inch diameter speaker cone. Left: Vibrating at 800 cycles per second. Right: Vibrating at 10,000 cycles per second. The contours of these pictures give the difference in position of the cone at the instants of the two exposures. This technique has advantages over time averaged interferometry in that it is capable of handling large excursions, can deal quantitatively with transient and non-sinusoidal events, and can give records of displacement at a given instant thus relating positions to other quantities such as coil current.

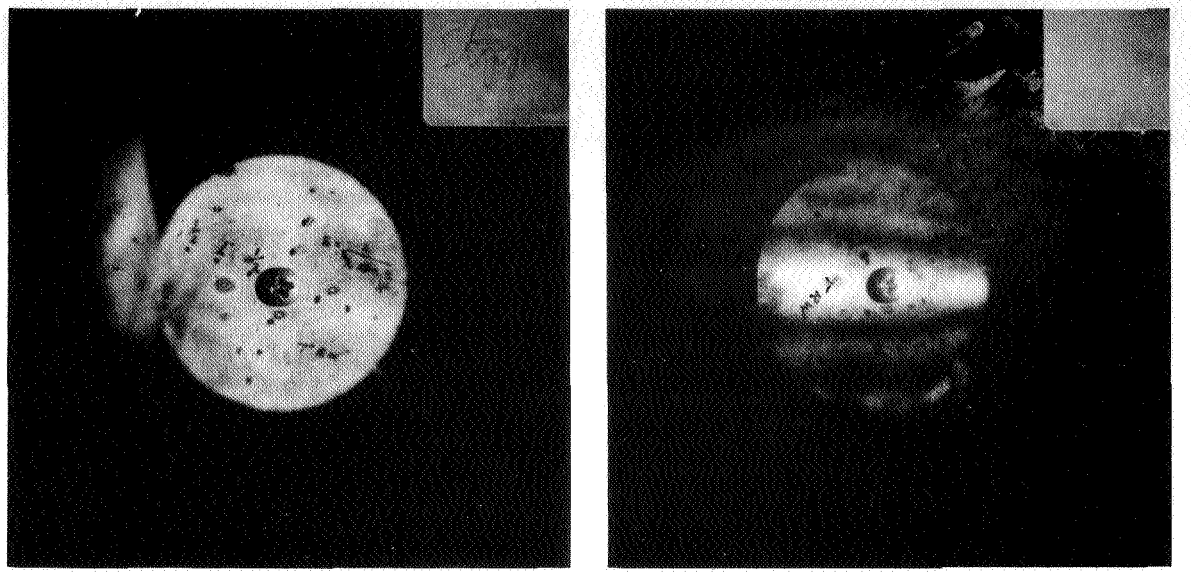

Fig. 3-4. Two photographs of a paper disk showing in a qualitative way the sensitivity of the reflected light holograms to motion. For the left picture the disk was stopped. For the right picture the disk was rotating at 1920 RPM giving a peripheral speed of 4 microns per microsecond. The geometry of the holocamera is such that primarily the horizontal component of motion is sensitive, giving the horizontal dark bands where the motion has time averaged the exposure during the approximately one-half microsecond duration of the single exposure.

4.0 TESTS IN LOW DENSITY CHAMBER

During this program, a small chamber was built in order to test the holographic interferometric camera with bullets in low density gas. The chamber, shown in Fig. 4-1, is simple in construction, consisting of a 4.5 in. length of 7.5 in. diameter aluminum pipe, to the ends of which are fastened 0.5 in. thick plexiglas sheets as windows. The bullet enters and exits through holes in the side of the pipe which are covered with 5 mil polyethylene membrane. All seals are made using O-rings so the chamber can be evacuated to a few microns pressure without leaking. The chamber is placed in the holocamera between the photographic plate and the condenser lenses with both reference and scene beams passing through it.

In operation the bullet travels 28 inches after leaving the barrel before entering the chamber. Fig. 4-2 shows some copies of holographic interferograms made with the chamber. Some show a piece of polyethylene from the entrance diaphragm traveling beside the bullet. All shots are in air. The pressures range from atmospheric down to 6 mm Hg. The shock front and some structure was visible in all shots of 50 mm or higher pressure. At 22 mm the shock layer can be seen from certain viewing directions, but not from others. In a 10 mm shot the shock layer was not visible.

The 6 mm shot shown in Fig. 4-2 is somewhat of an anomaly. There apparently was a small movement of the apparatus between exposures which introduced "finite fringes." These fringes, of which there are only two, are the dark elliptical region to the left and slightly above the bullet, and the curved dark fringe on the right side and the bottom. The portion of the shock front which is visible runs through the dark elliptical "fringe." The visibility of the shock front is maximum somewhere near the quarter wave region. This is not unexpected and is an accidental crude approximation to the sub-fringe interferometry technique.

The general quality of the holograms shown in Fig. 4-2 is not up to the best we have achieved before. In our eagerness to try the new chamber, we apparently failed to align the laser and holocamera to its best performance. This is manifested by the non-uniform background evident in the pictures.

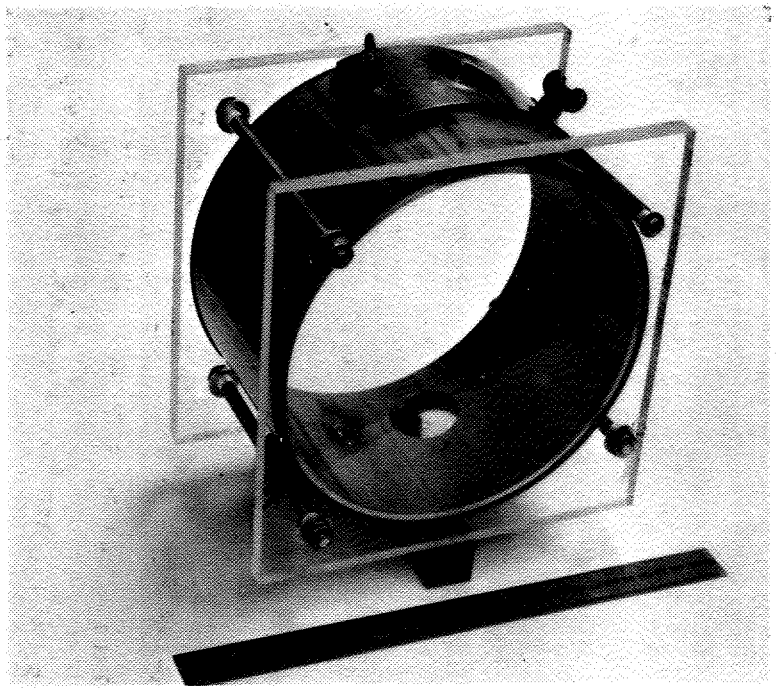

Fig. 4-1. Low density chamber used for holographing bullets in flight in gases at sub-atmospheric pressures.

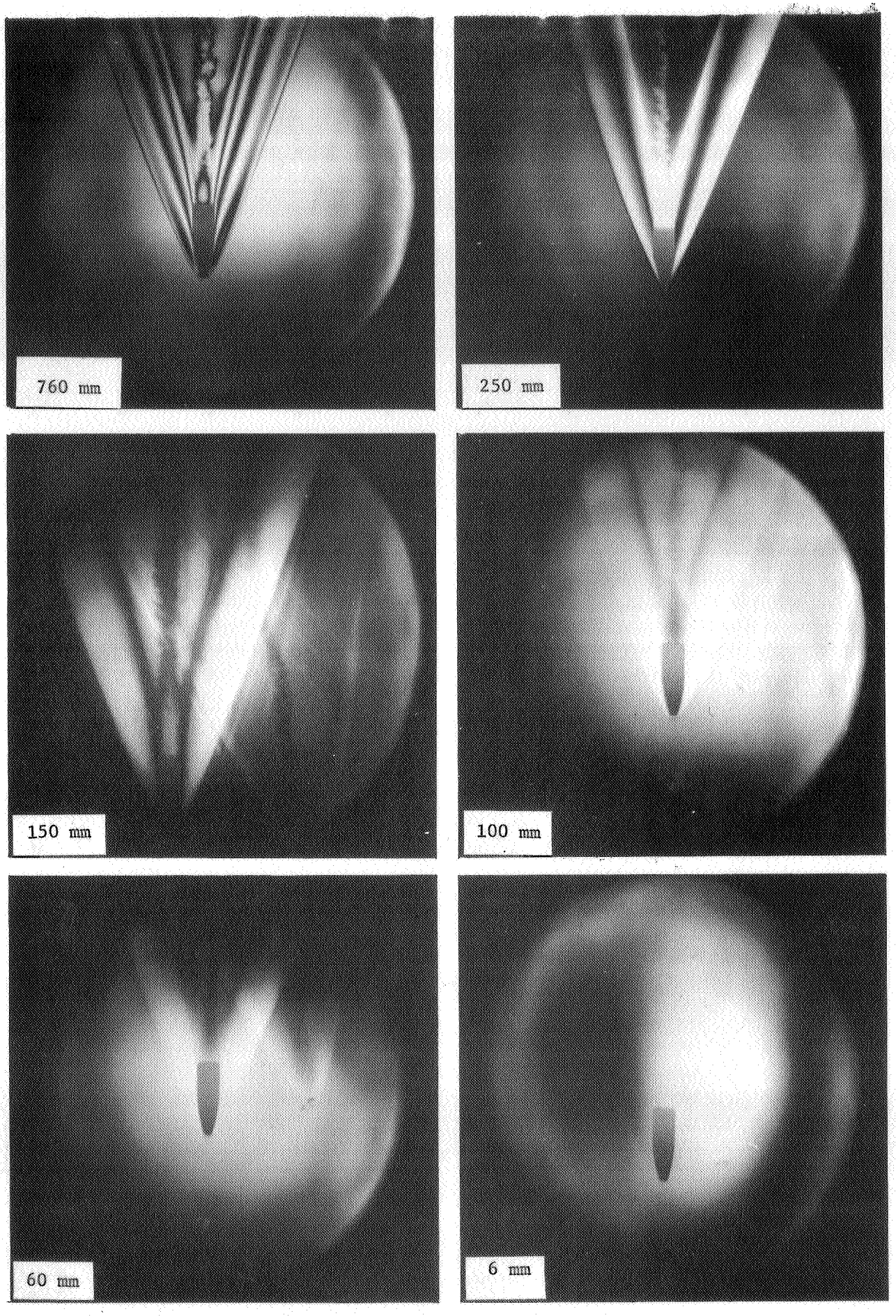

Fig. 4-2. Copies from holographic interferograms made in the low density chamber. Air pressures in mm Hg are given for each picture.

5.0 SUB-FRINGE INTERFEROMETRY

Experimentation has begun in an attempt to render consistently available the sensitivity fortuitously manifested in a portion of the 6 mm shot of Fig. 4-2. Shown in Fig. 5-1 is a gas cell phase shifter which permits the phase of the scene beam light to be accurately shifted between the two exposures of an interferogram.

The gas cell itself consists of a cylindrical chamber 0.95 cm in length and 3 cm diameter. The air pressure in this chamber is set to one atmosphere for one of the exposures, and for the other exposure the air pressure is reduced by an amount appropriate to produce the desired phase shift. The pressure is monitored by a long water manometer. A decrease in pressure of 133 centimeters of water produces a half wave decrease in optical path.

The gas cell was first tried in the scene beam of our pulsed ruby holocamera. For the test the pressure difference was set to produce a half wave change. This should have resulted in a near blackout of the scene. Repeated tests failed to produce the expected blackout.

In order to understand these unexpected results, the gas cell was tried in a gas laser holographic setup, the same one used to evaluate the finite fringe technique. There it was found that room vibration and/or air turbulence were probably responsible for the failure of the tests with the pulsed holocamera. Even with the gas laser setup on a granite table, these factors produced occasional failures.

Fig. 5-2 shows successful operation of the gas cell in the gas laser setup. The top picture shows a finite fringe picture through the gas cell. By laying a straightedge on the print, one can see that the phase shift is approximately one-half wave. The lower picture is closer to the intended use of the gas cell. In this case, the hologram was made with a double exposure, the cell pressure being given a half-wave shift between exposures. The dark interior of the cell shows the expected phase cancellation.

In actual operation to produce sub-fringe interferograms, the gas cell will be placed in the beam illuminating the ground glass, instead of in front of the ground glass as in Fig. 5-2.

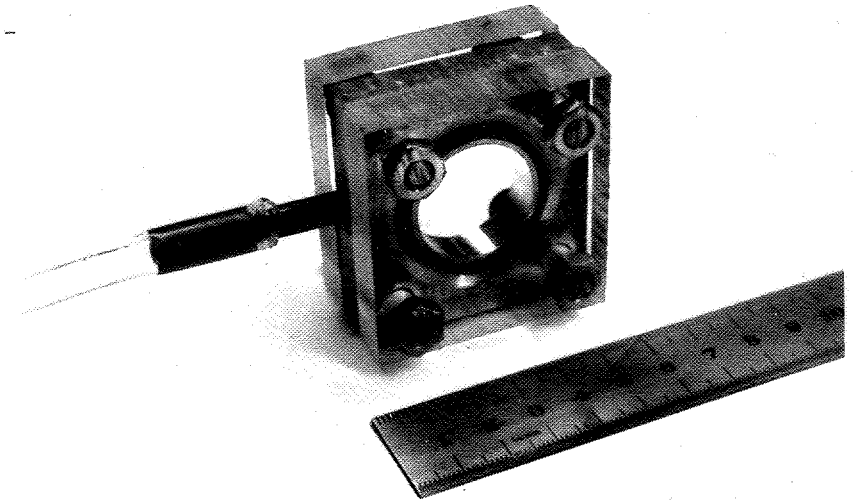

Fig. 5-1. Gas cell phase shifter used to produce controlled phase shifts for sub-fringe interferometry.

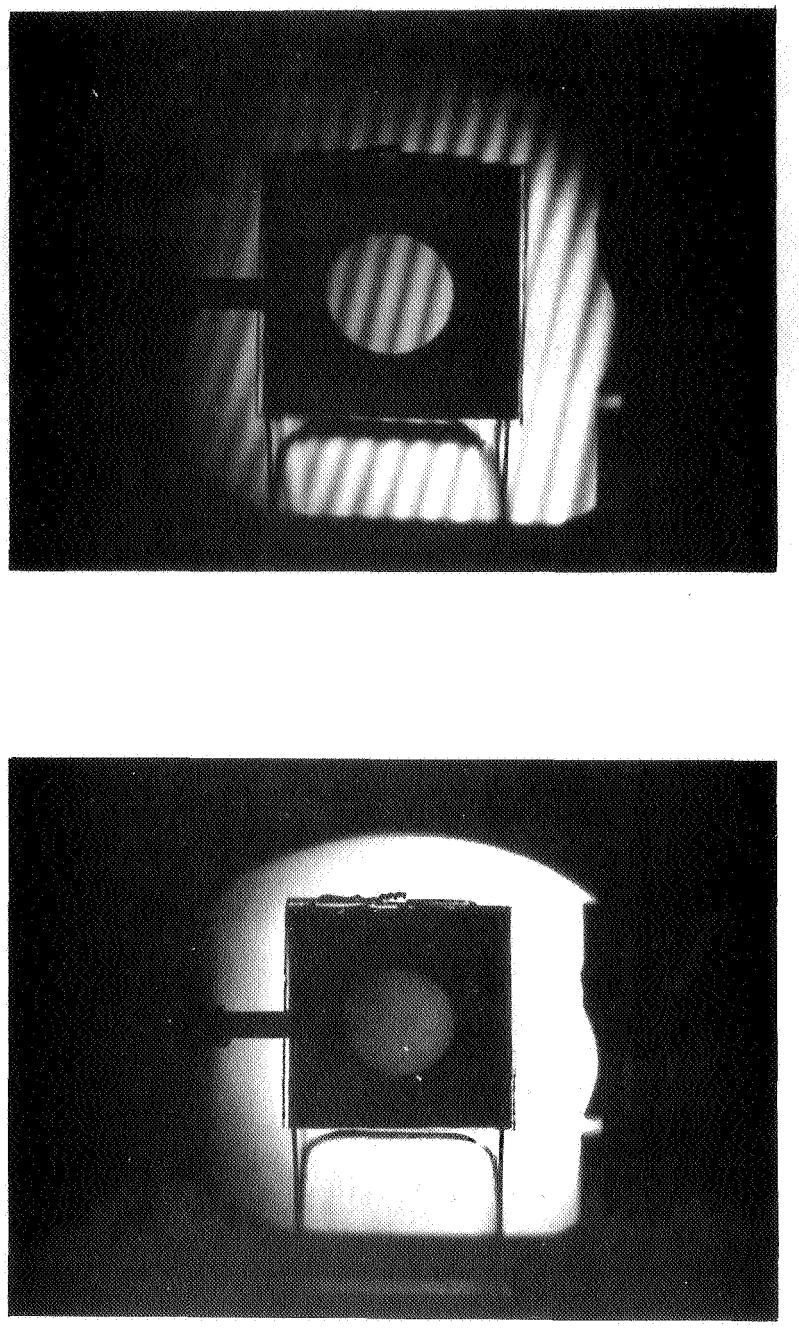

Fig. 5-2. Copies from gas laser test interferograms using the gas cell phase shifter. In both holograms the gas cell shifted the phase 180°. Upper: A finite fringe hologram with fringes focused in the plane of the gas cell. Lower: A double exposure hologram showing the cancellation within the cell from the 180° phase shift.

The adjustment of the gas cell to produce a maximum of sensitivity is a matter requiring further experimentation. A phase shift of 90° can be shown to create the maximum absolute change in intensity associated with a small perturbation of the phase by the subject. However, it is not clear that maximizing the absolute change of the intensity will maximize the visibility of small changes. In contrast, consider maximizing the ratio $\frac{\Delta I}{I}$, where I is the intensity. To maximize this ratio, the phase shift should be set at 180° so the two exposures cancel each other in absence of subject perturbation. With such a null or black background, very small subject phase shifts should produce detectable brightenings. This concept of null interferometry has probably occurred to others using classical interferometry, and since it is not in general use it is appropriate to ask why it is not and then to see if the new freedom permitted by the holographic techniques makes possible a practical system.

To secure a good null requires that the intensities of the two interfering beams be nearly equal over the entire scene and also that the relative phases be close to 180° over the entire scene. In the holographic case, it is the two exposures (= intensity x time) that need to be equal. These requirements are very severe and perhaps the lack of use in the classical case may be attributed simply to the severity of these requirements.

Due to the common path nature of holographic interferometry, wherein a beam is compared to itself at a later time, it would seem that it may be easier to achieve the above requirements, offering some hope for a workable system.

However, the holographic process introduces new uncertainties. For example, it is not known to what extent two holographically recorded wave fronts can be made to cancel. In Fig. 5-2, lower, it is clear that there is cancellation, but it is also clear that the cancellation is not very complete. It was estimated with neutral density filters that the canceled window is about one-tenth as bright as the surrounding region where no phase shift took place. It is not known at present whether better cancellations can be obtained.

A simple mathematical derivation, given in Appendix I, shows that the phase sensitivity is proportional to the square root of the blackness of the null. Because of this, we are not highly optimistic for the technique.

A reason to expect non-perfect cancellation in holographic systems utilizing a ground glass in the scene stems from the statistical nature of the "granularity" pattern at the hologram plane. In systems incorporating a diffuser, it can be shown from the central limit theorem that the probability that the scene light intensity is greater than R times the average intensity, at a random selected point of the hologram plane, is e^{-R}. The occasional large excursions in intensity predicted by this formula show that there will be places on the hologram where the linear behavior of the hologram will be clipped. Thus, the reconstructed wave must be an imperfect copy. The effect of this clipping is to produce diffusely scattered light, which therefore interferes with the production of complete cancellation giving very black nulls.

10347

6.0 FINITE FRINGE HOLOGRAPHIC INTERFEROGRAMS

The type of interferogram which is normally produced by holographic interferometry is the "infinite fringe" interferogram. Such interferograms result when there are no changes between the two exposures other than those associated with the subject. If a small movement of the apparatus takes place between the two exposures, then the background of the reconstructed scene will be covered with interference fringes, usually approximately straight and parallel to each other. These fringes have an appearance very similar to the finite fringe interferograms of conventional interferometry. However, there is an important aspect of the holographic case which requires further consideration ; the holographic image is three-dimensional and the interference fringes can appear to have a specific location in space. For certain practical applications, it is desirable to be able to place these fringes in the plane of the subject.

As an example, Figure 2-6 shows a photograph of a finite fringe holographic interferogram made by introducing a small motion between exposures. The quality of this copy was poor because the fringes were located approximately at infinity, which made it difficult to have both the fringes and the bullet in focus at the same time. A small aperture was used to make the photograph, but the coherence granularity places a limit on one's ability to increase depth of field in such a fashion. In order for such a picture to be useful for the quantitative evaluation of small details, it is necessary that the background fringes focus in essentially the same plane as the subject.

To solve the problem of deliberately placing the finite fringes in a desired plane, a formula has been derived which gives the location of the fringes in terms of the movement imparted to the ground glass and the directions of viewing and illumination.

In order to maintain simplicity, the arrangement considered is basically a two-dimensional system. As will be shown, the experimental tests demonstrate that the result can be used to locate the fringes in certain actual three-dimensional arrangements, even though the analysis is two-dimensional.

Fig. 6-1 shows the geometry of the arrangement studied. In practice, the diffusing surface stands perpendicular to the plane of the paper. However, the analysis considers only the rays which lie in the plane of the paper. The motion permitted of the ground glass is any combination of translations and rotations in the plane of the paper. That is, the ground glass remains perpendicular to the plane of the paper, but is otherwise free to move in any manner as a rigid body.

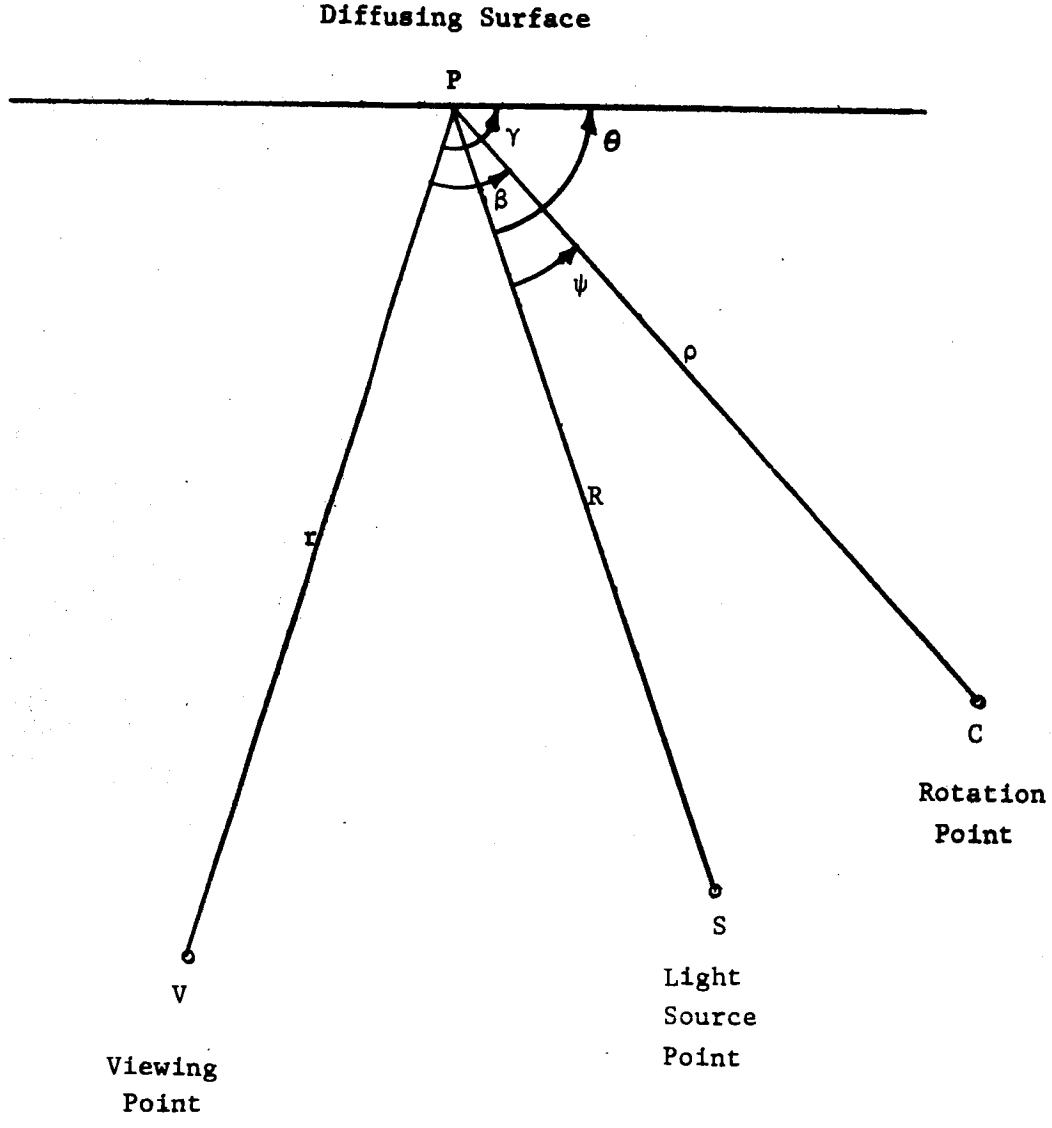

Figure 6-1. Geometry for the location of finite fringes.

Now any combination of translations and rotations of the ground glass can be described simply as a rotation about a certain point in the plane. This rotation center is denoted by point C in the diagram, and the angle of rotation about this point will be denoted by δ. (If the motion is a pure translation, the point C is at infinity). Also shown is the point source, S, from which the illuminating light diverges and the point V where the viewer's eye is located. The point P is an arbitrary point on the diffusing surface. The hologram is located between the diffusing surface and the viewer's eye. Its particular position is not important, and also the particular arrangement used for the holographic reference beam is not important. The hologram simply serves as a storage mechanism for the light waves produced at two different times, allowing both light wave patterns to be simultaneously reconstructed.

The distances from P to the viewing point, illumination source point, and rotation point are denoted by r, R and ρ respectively, as shown in the diagram. The angles these points subtend from the point P are denoted as follows:

β = angle from viewing point to rotation point

γ = angle from viewing point to surface

θ = angle from source point to surface

ψ = angle from source point to rotation point

These angles may take on any value from 0 to 360°. In terms of these parameters, the distance f from the point P to the focus of the interference fringes is

$$f = (\rho\cos\beta)\,\frac{1}{1 + \frac{\sin\theta}{\sin\gamma}\left[1 - \frac{\rho\cos\psi}{R}\right]} \qquad (1)$$

That is, as one looks in the direction of point P from V, the fringes appear to be a distance f in front of the ground glass on the line joining P and V. (If f is negative, the fringes appear to be behind the ground glass.) As the point P moves across the ground glass, formula (1) can be used to plot the surface on which the fringes appear to lie. Notice that the first factor, $(\rho\cos\beta)$, is the distance from P to the foot of the perpendicular projection of the rotation point C on the viewing line.

The spacing S of the fringes in their focal plane is given by the formula

$$S = \frac{\lambda}{\delta}\left(1 - \frac{f}{r_0}\right) \frac{1}{1 + \frac{\sin\theta}{\sin\gamma}\left(1 - \frac{\rho\cos\psi}{R}\right) - \frac{\rho\cos\beta}{r_0}} \qquad (2)$$

where r_0 is the distance from the observer's eye to the point P.

Formulas (1) and (2) are derived in Appendix II.

The formulas were used as a guide in setting up an experiment to see if the finite fringes could be placed in a desired subject focal plane. The experiment served also to evaluate the formula's effectiveness in a real three-dimensional situation in contrast to the two-dimensional analysis.

The desired objective was to place an array of fringes which focus in a plane at the location of the subject. The subject location is between the viewer and the ground glass.

The test was also arranged so the light passed through the ground glass, which is the situation most useful for the interferometry of aerodynamic scenes. γ was chosen as 90° for the center of the ground glass, thus the sensitivity to change in γ for different points on the ground glass is minimized. For a similar reason, R was chosen as infinity, that is, parallel light illuminated the ground glass. It would have been natural to have the illumination perpendicularly incident on the rear of the ground glass, but the formula shows that the fringes would then focus at infinity due to the cancellation occurring in the denominator of (1). Consequently, θ was moved off perpendicularity. The angle $\theta = -58°$ was chosen, which permitted an available prism plate to be used to direct the bulk of the scattered light toward the viewer. The prism plate was attached to the ground glass and moved with the ground glass. These choices gave the value of the fraction in (1) as 6.6. The rotation point was located on the observer's side of the ground glass along a line passing through the mid-line of the ground glass. Two values of ρ were used. The longer value of 9 cm gave fringes located 60 cm from the ground glass, in quantitative agreement with the formula. The shorter ρ value of about 2 cm gave fringes at 10 cm from the ground glass. The agreement is

considered satisfactory in view of the uncertainty in determining the effective location of the ground glass-prism plate combination.

The rotational motion was imparted to the ground glass by mounting it on a metal bar at distance ρ from a knife edge pivot at the end of the bar. A 2-56 screw and spring at the other end of the 1/2 meter long bar imparted the controlled rotation to the bar. The spacing of the observed fringes was in agreement with the value given by formula (2) within the crude precision of the experiment, say ± 50%.

Fig. 5-2 is a photograph of a holographic image containing a finite fringe pattern which focuses in the plane of the subject. The hologram was made in the geometry described above. The subject in this case is a small gas cell used to produce controlled phase shifts as described elsewhere in this report. The fringes focus accurately in the mid-plane of the cell. When the observer of the hologram moves his head from side to side, there is essentially no relative motion between the fringes and the cell.

Fig. 6-2 (a, b, c) attempts to show the focusing property of the finite fringes. In this example, there are three wires separated in distance along the viewing direction by approximately one inch. The copy camera was focused on these three different wires in a, b, and c. The finite fringes are approximately in the plane of the wire, which is in focus in c. One can see from a that the fringes are considerably reduced in contrast when the wide aperture copy camera was focused 2 inches in front of the fringe focal plane.

The tests described have demonstrated that it is possible to deliberately place a set of finite fringes in a holographic image at a selected focal plane. This makes available to the aerodynamicist the same finite fringe patterns which he is accustomed to in conventional interferometry. In the holographic case, however, there is still three-dimensional information available insofar as the holographic image permits a wide viewing angle. The practical usefulness of this three-dimensional aspect is an area that still remains to be exploited.

One area where the finite fringe holographic interferogram may find application is in cases where the subject causes fringe shifts of only a small

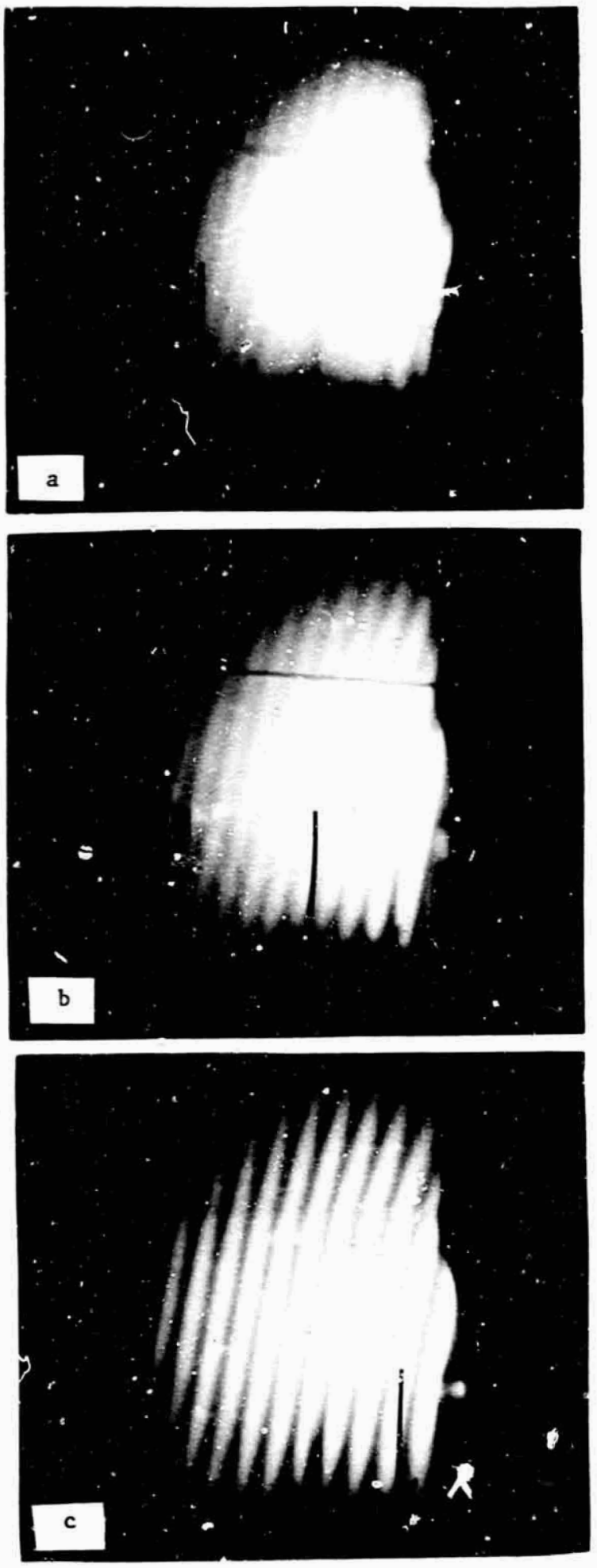

Fig. 6-2. Copies from gas laser holograms showing the focusing ability and placement of finite fringes. The three different wires in focus in a, b, and c are separated by about one inch in depth. The fringes focus in the plane of the wire in c.

fraction of a fringe. In this case, the precise location of the unperturbed fringes is important, for it is the deviations from this position that are important. In classical interferometry, the unperturbed fringe position depends on the optical quality, and it is difficult to produce truly smooth fringes over a large aperture. In holographic interferometry, the fringes are produced by a rigid motion of the ground glass, with complete insensitivity to the optical quality of the components. This insensitivity to the optical quality may make possible a more accurate determination of fringe shifts caused by the subject.

The application of the above finite fringe techniques to holographs of bullets in flight has not been accomplished yet due to the increased complexity of the holographic configuration required for the pulsed ruby laser.

7.0 INTERFEROMETRY WITH DOUBLED RUBY RADIATION

The following article, reproduced from Applied Physics Letters, Vol. 12, No. 9, May 1, 1968, describes an experiment with ultraviolet light for increasing the sensitivity of holographic interferometry.

HOLOGRAPHIC INTERFEROMETRY WITH ULTRAVIOLET LIGHT*

R. F. Wuerker, L. O. Heflinger, and R. A. Briones
TRW Systems
Redondo Beach, California
(Received 13 March 1968)

Simultaneous red and ultraviolet holographic interferograms were recorded on a single Eastman 649F plate by radiation existing after the passage of a Q-switched ruby laser beam through a KDP crystal. The ultraviolet record had twice the sensitivity to optical path length changes as the red record.

Holograms have been made with ultraviolet radiation. The radiation was obtained by second harmonic generation in a KDP crystal fed with red light from a Q-switched ruby laser.

One reason for interest in holograms made with ultraviolet light is that the shorter wavelength doubles the number of fringes in holographic interferograms, rendering smaller changes visible.[1] Figure 1 shows an example of a double-exposed holographic interferogram. This holographic interferogram was made by exposing the plate once with the lamp filament cold and a second time with the lamp filament heated to a dull glow, causing density changes in the heated filling gas. The new aspect of this hologram is that it is simultaneously two holograms, one made with the red light component (6943 Å) and one made with the harmonic ultraviolet component (3471 Å). In the red picture (left), only one fringe is visible. Two fringes are seen in the ultraviolet reconstruction due to the shortened wavelength.

Since both reconstructions were obtained with the 0.6328-μ beam from a He-Ne laser, the angle at which the uv reconstruction occurs is approximately double that of the red reconstruction. As a result, the two could be separately photographed.

The hologram arrangement and laser used in these tests was essentially identical to that described in an earlier paper.[2] The laser illuminator consisted of a $\frac{1}{2}$"-diam by $3\frac{3}{4}$"-long 60° ruby rod of high homogeneity, a nitrobenzene Kerr cell Q switch, an air-spaced Glan polarizer, and a 1-cm-diam intercavity aperture. The optical resonator consisted of a 99% reflectivity, dielectric-coated optical flat and an output sapphire resonant reflector, separated by 1.5 m. This laser emitted a single $\frac{3}{4}$ J pulse of red radiation of 50 nsec duration—enough to record a hologram on a full 4 × 5 in. 649F plate.

The output of the laser was passed through a KDP doubler[3] oriented to maximize the generation of ultraviolet radiation. Tests showed that the energy conversion efficiency was 5%. The ultraviolet alone was sufficient to expose the full 4 × 5 in. area of the plate.

The combined beam from the laser was expanded by a simple lens of −5 cm focal length, then divided into "scene" and "reference" beams by an elementary holocamera consisting of a glass beamsplitter and three front surface mirrors.[2] A ground glass was placed in one beam ~13.5 cm from the photographic plate. The light bulb scene was placed between the plate and the ground glass screen. Red-only holograms were made by placing a pair of Corning CS7-60 glass filters before the output of the doubler, which absorbed 99% of the ultraviolet radiation without damage. Ultraviolet-only holograms were made with a pair of Corning CS-2-58 red absorbing filters. For simultaneous red and uv holography, plates of window glass, partially absorbing in the uv, were placed at the output of the doubler to balance the relative exposure, thereby equalizing the brightnesses of the two reconstructions.

The quality of the hologram was poor because spatial matching techniques could not be fully exploited due to the nonavailability of ultraviolet transmitting lenses.[4] The quality of the reconstruction is essentially identical in the red and uv, and similar to earlier results with this type of simple system.[2]

An interesting observation made while viewing the hologram is that the angular orientation sensitivity of the plate is less for the uv (±23°), than it is for the red (±11°). This difference is apparently due to the absorption of the gelatin rendering the effective thickness of the emulsion only 2.5 μ in contrast to the 11 μ full thickness of emulsion utilized by the red.

The results demonstrate that doubling the ruby light is a practical method for gaining a factor of two in the sensitivity of holographic interferograms. By constructing a holocamera with optics transparent in the uv, good quality interferograms should be possible.

*Work for this research was jointly sponsored by the Air Force Rocket Propulsion Laboratory (Contract F04611-67-C-0105) and the National Aeronautics and Space Administration Headquarters (Contract NASW-1572).

[1] L. O. Heflinger, R. F. Wuerker, and R. E. Brooks, *J. Appl. Phys.* **37**, 642 (1966).

[2] R. E. Brooks, L. O. Heflinger, R. F. Wuerker, and R. A. Briones, *Appl. Phys. Letters* **7**, 92 (1965).

[3] Korad Model K-M frequency doubler with 1-in.-thick crystal cut at 55° relative to crystal axis.

[4] R. E. Brooks, L. O. Heflinger, and R. F. Wuerker, *IEEE J. of Quantum Elect.* **QE-2**, 275 (1966).

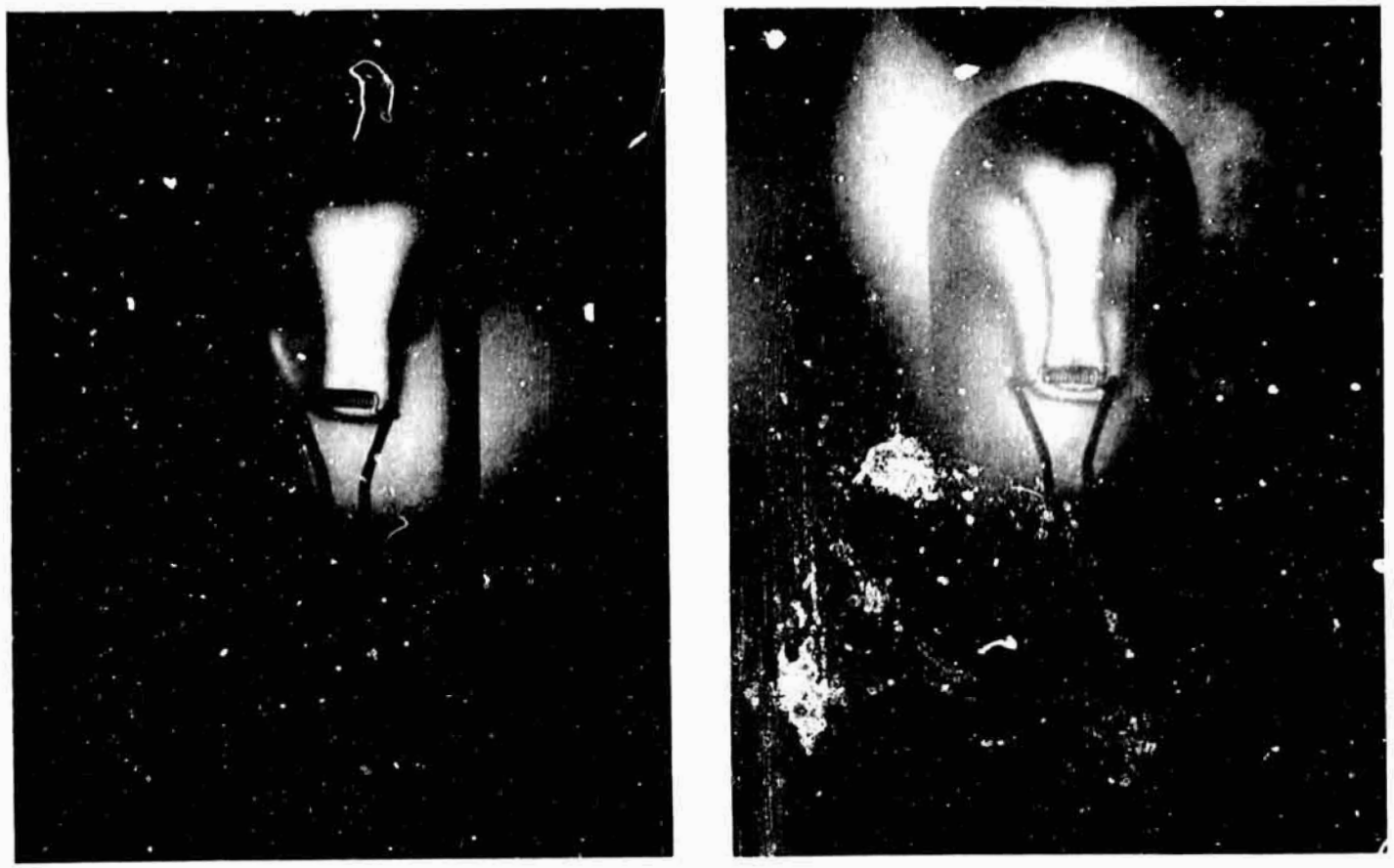

Fig. I. Photographs of the two reconstructions from a single holographic interferogram of a projection lamp. The hologram was exposed simultaneously by the doubled and primary radiation from a Q-switched ruby laser. The filament of the lamp was heated between the two exposures, producing optical path length changes in the filling gas. Both images were reconstructed with a helium neon laser. The 0.6943 micron image is on the left. The other is the 0.347 micron or "doubled" image.

8.0 HOLOGRAPHIC INTERFEROMETRY USING HIGH ORDERS OF DIFFRACTION

8.1 Introduction and Summary

By using the light diffracted into orders higher than the first, the phase sensitivity of holographic interferograms can be increased over the first order sensitivity by a factor equal to the order number used. The following discussion gives the results of an investigation made to determine the practical usefulness and limitations of interferometric techniques based on the above principle. The fundamentals of the process will be given and a useful holographic method will be described which has been experimentally found to give a factor of 4 increase in sensitivity while still retaining the usual holographic advantages of the ability to function through imperfect optics without precision alignment. A simple mathematical analysis is given which describes the behavior of the system and which shows the influence of exposure variations on the performance of the system.

8.2 Basic Principle

The basic principle that the light diffracted into the nth order from an interferogram has n times the phase variation of the exposing wave will now be described.

Consider a configuration in which two parallel beams of monochromatic light impinge at an angle θ on a photographic plate (Fig. 8-1).

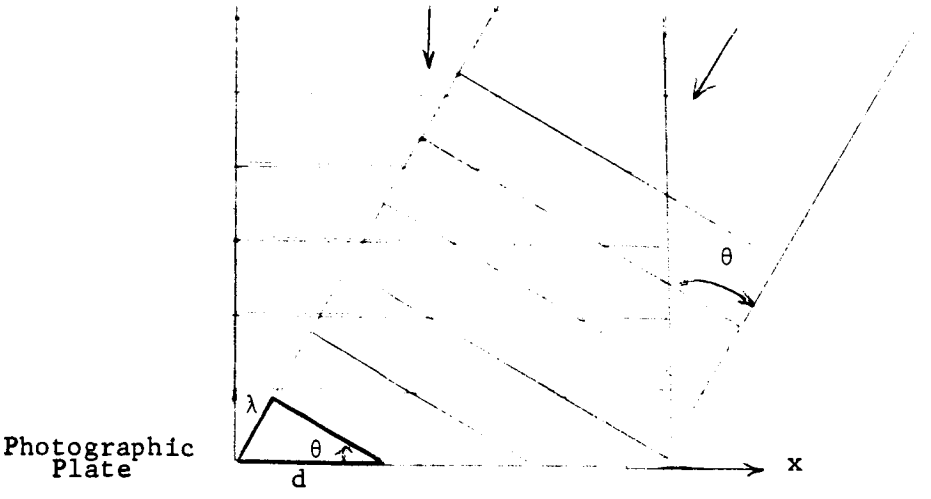

Figure 8-1

At the photographic plate, intensity maxima and minima are produced where the two waves are respectively in phase and out of phase. This results in the photographic plate being exposed in a set of lines perpendicular to the plane of Fig. 8-1 with a spacing given by

$$d = \frac{\lambda}{\sin \theta}$$

(Here it is assumed for simplicity that one beam is perpendicular to the photographic plate.)

Now if a phase object is placed in one of the beams, then for each point of the plate the location of the intensity maxima will be shifted on the plate by an amount proportional to the phase shift along the ray passing through that point of the plate. Specifically, a phase shift of ϕ radians produces a lateral shift of the fringe pattern by a distance of $\frac{\phi}{2\pi} d$. (The situation described so far does not differ from that of a classical finite fringe interferogram.)

Next we consider the effect produced by the phase shift ϕ when the photographic plate, exposed in the foregoing manner, is used as a diffraction grating (i.e., hologram). Fig. 8-2 shows the diffraction process. Here, again for simplicity, the incident monochromatic light is perpendicularly incident on the photographic plate.

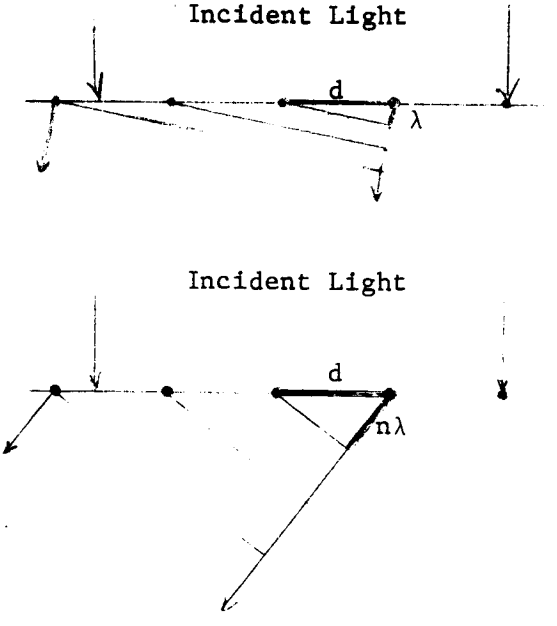

Figure 8-2

Fig. 8-2a shows light being diffracted into the first order. Fig. 8-2b shows light being diffracted into the nth order. From this figure, one sees that if the fringes on the photographic plate are moved a distance d, then the phase of the nth order diffracted light is shifted n wavelengths, i.e., by an angle of $2\pi n$. Thus, letting Δ denote the fringe displacement, the phase shift in the light diffracted into the nth order is $2\pi n\frac{\Delta}{d}$. But, from the earlier discussion, the displacement Δ in fringe position due to a phase shift ϕ during exposure has been shown to be $\Delta = \frac{\phi}{2\pi} d$. Combining this gives the result that in the nth order diffracted wave, a phase shift of $n\phi$ results from a phase shift of ϕ during exposure.

Note that the result also holds for orders on the opposite side of the zero order, the n in this case being negative, and the resulting phase shift being of opposite sign to the phase shift of the original perturbation.

8.3 Utilization of the Basic Principle

There are many ways in which the basic principle may be applied in attempts to gain increased sensitivity from interferometers. We shall first describe some schemes which readily occur and shall comment on their properties.

Perhaps the simplest scheme conceptually is a form of stored beam interferometer. For example, if a single exposure is made with a phase subject in place in one of the beams of Fig. 8-1 and then the nth order reconstruction from the developed hologram is used to create a beam as in Fig. 8-2 with the n-fold increase in subject phase perturbations, these phase variations can be turned into intensity variations by interfering the nth order output beam with a plane wave which is superimposed on the nth order beam by a beam splitter.

A variation of the above scheme would be to bring the nth order reconstructed beam into approximate coincidence with the -nth order beam by means of mirrors and beam splitters. The interference between these two beams would result in a 2n-fold increase in sensitivity.*

The immediate objection to these systems is that they require beams whose wavefronts are flat to a fraction of a wave. That is, there is no self-comparison,

---

* Such a scheme is somewhat akin to the Three Beam Technique of M. De and L. Sevigny (Applied Physics Letters 10, No. 3, 1 Feb. 1967, p. 78). They use three beams during exposure, with the result that upon reconstruction the +1 order from one pair interferes with the -1 order from another pair, giving a single exposure holographic interferogram of double sensitivity.

as with the usual holographic interferometry, that results in insensitivity to the perfection of the optics and alignment.

In an attempt to achieve these desirable self-compensating properties of holographic interferometry, we consider next the double exposure process of holographic interferometry. In this process, two exposures are made on the same plate, one with the subject absent and the other with the phase subject present. After the exposures, the plate is developed and then reconstructed. The light diffracted into the first order then has an intensity pattern which is similar to the intensity pattern which would have been produced had the two exposing beams--scene present and scene absent--somehow existed at the same time and interfered with each other. The absence of requirement for precision optics and alignment stems from this comparison of the subject-perturbed beam to the same beam without the subject.

If one applies the above process and then looks in the second or higher orders of diffraction, the interference pattern observed is the same as that observed in the first order. That is, the method does not produce the desired phase multiplication in the higher orders. To understand this, consider the intensity at the photographic plate for the first exposure. It will have the form

$$I_1 = I_0 \sin^2 \pi \frac{x}{d} \quad , \tag{1}$$

where d is the fringe spacing as before. (Here equal intensity beams have been assumed for simplicity.) For the second exposure, the intensity is

$$I_2 = I_0 \sin^2 \pi \left(\frac{x}{d} + \frac{\phi(x)}{2\pi} \right) ,$$

where $\phi(x)$ is again the subject phase shift and is assumed to change slowly with respect to the fringe spacing d.

The exposure on the plate is proportional to the sum of the two intensities which by a little trigonometric manipulation may be written in the form

$$I_1 + I_2 = I_o \left[(1 - \cos \frac{\phi}{2}) + 2 \cos \frac{\phi}{2} \sin^2 \left(\pi \frac{x}{d} + \frac{\phi}{4} \right) \right] .$$

By inspection of this formula, it will be observed that when $\phi = 0, \pm 2\pi, \pm 4\pi, \ldots$, the exposure simply produces a grating as would a single exposure. However, for regions of the plate where $\phi = \pm \pi, \pm 3\pi, \pm 5\pi, \ldots$, the exposure is essentially constant and no grating is produced. This absence of a grating results in a black region in all orders, and in general the phase ϕ has simply modulated the efficiency of the basic grating. Experimentally, the diffraction efficiency is sufficiently similar in all orders so that one sees the same first order pattern in all orders.

Still another approach to the utilization of high orders is to make the two exposures of double exposure holographic interferometry on separate plates, and then to reconstruct them simultaneously by placing the plates one behind the other in the reconstruction beam.

Two separate cases may be considered. For the first case, consider the situation where the plates are well separated. Then the plates act as separate diffraction gratings, the second plate re-diffracting the light from the various orders of the first plate. In this case, for example, if one observes at an angle corresponding to the second order, one will actually see the superposition of light diffracted into the jth order by the first plate and subsequently diffracted into the (j-2)th order by the second plate. The superposition extends over all orders j. This results in a mixture of orders being observed at a given output angle, and experimentally has been found to give patterns too complex to be easily interpreted.

The second case is where the two emulsions are placed in contact. Here a single diffraction takes place from the superposition of the two gratings. It is this case, coupled with some refinements to be described, that yields a practical system. At this point, we shall digress to incorporate these refinements before describing the behavior of this system in detail.

8.4 The Production of Narrow Fringe Lines

The ability to produce fringe lines which are a small fraction of the fringe spacing is important to the process in two ways. The primary reason is that two exposures can then be superimposed with a minimum of undesirable interaction as will be seen presently. The other reason is that in practice, narrow lines diffract the light more uniformly into the higher orders, facilitating the readout process.

There is a simple method for producing narrow fringe lines. It consists of nothing more than heavily overexposing a high contrast plate during the original exposure, and of making sure that the two beams are nearly equal in intensity. The heavy exposure blackens the entire plate with the exception of fine lines where the relative phases of the two beams are out of phase.

We next establish the relationship between the exposure and the ratio of the clear width to the fringe spacing in the case of an ideal film. If one had a film with infinite gamma, that is, a film that turned from clear to opaque whenever a certain exposure threshold was exceeded, then the ratio η of the clear width to the fringe spacing, derived from Equation (1), would be

$$\eta = \frac{2}{\pi} \sin^{-1} \sqrt{\frac{\varepsilon_{50}}{2\varepsilon}} \quad ,$$

where $\varepsilon/\varepsilon_{50}$ is the ratio of the exposure to that exposure which produces 50 percent clear fringes. For very heavy exposures, the case of present interest, the above can be simplified to

$$\eta \cong \frac{\sqrt{2}}{\pi} \sqrt{\frac{\varepsilon_{50}}{\varepsilon}} \quad . \tag{2}$$

Thus, for example, exposing 20 times that which produces 50 percent fringes produces clear spaces of one-tenth the width of the fringe spacing.

The preceding formulas assume equal beam intensities, and it is appropriate to estimate the equality required for the formulas to be useful. If the ratio of the two beam intensities is denoted by $1 + \delta$, then for small differences in intensity, the ratio of minimum intensity to average intensity is $\frac{\delta^2}{8}$ and the above formulas will be valid provided $\frac{\delta^2}{8}$ is small compared with $\varepsilon_{50}/\varepsilon$. This is a surprisingly easy requirement to satisfy, for instance, using the above example, if $\delta = .1$ (intensities different by 10%), then $\frac{\delta^2}{8} = .00125$, which is small compared to $1/20 = .05$. Thus, the required beam intensity ratio is easy to satisfy in practice.

Available films fall short of the ideal gamma used above; nevertheless, we have experimentally obtained gratings with ratios up to 1:10, clear width to grating spacing, with Kodak 649F emulsion and also with Kodak Kodalith Pan emulsion. Even higher ratios are possible, but the sharpness of the edges and

clarity of the clear regions decreases, limiting the usefulness. Fig. 8-6b and 8-8a show photomicrographs of fringes produced with a CW He-Ne laser, 6328 Å. The ratio of clear width to grating spacing is approximately 1:10 in these photomicrographs.

If we were to make our two exposures on separate plates, one with subject and one without subject, and were then to place these emulsions in contact, it is clear that for small values of η, the superposition will be opaque almost everywhere. This problem is avoided by reversing the clear and opaque regions by contact printing. The superposition is accomplished by contact printing both original exposures on the same plate.

8.5 A Useful Process for Producing Holographic Interferograms Capable of High Order Readout

Now that the general approach has been outlined, we shall restate for clarity the steps for the production of holographic interferograms which are capable of high order readout and which retain the usual holographic advantages of absence of requirement for precision optics and alignment.

The arrangement for the formation of the holograms consists of two beams from the same laser source impinging at a small angle on the hologram so that moderately coarse fringes (say a fraction of a millimeter) are produced. The Mach-Zehnder and Michelson arrangements are convenient for this purpose for they permit the subject to be easily placed in one of the beams while avoiding long paths between subject and hologram. Interferometric accuracy is not required for the components nor the adjustment.

Step 1. Make a heavily exposed hologram of the empty scene.

Step 2. On a second photographic plate, make a heavily exposed hologram with the phase subject in place in one of the beams.

Step 3. On a third photographic plate, make a double-exposed contact print of the holograms made in steps 1 and 2, one exposure from the hologram of step 1, the other exposure from the hologram of step 2.

Step 4. Reconstruct the contact print of step 3 with a laser and view the light diffracted into the nth order. A lens and aperture near the focal point are useful in isolating the light of a particular order, as shown in Fig. 8-3.

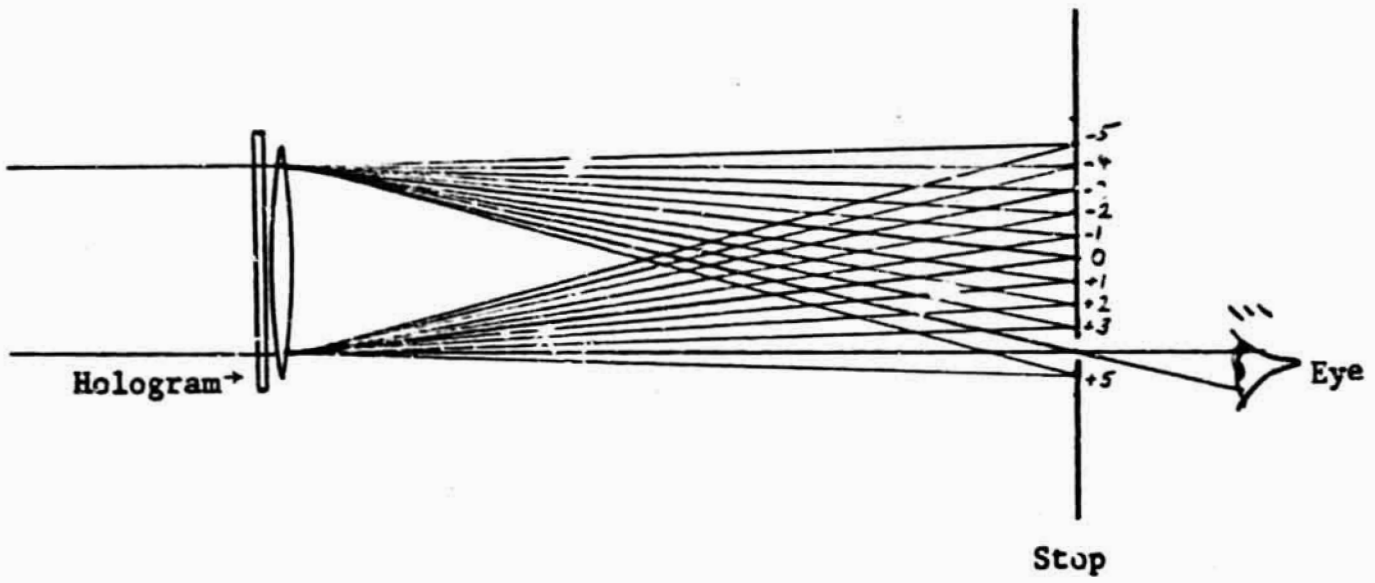

Figure 8-3

The intensity variations viewed by the observer correspond (with limitations to be stated later), to the intensity variations of conventional interferograms of the subject except that the phase sensitivity is n times as great.

8.6 Analysis of the Performance of Interferograms Produced According to the Above Process

In the following, the intensity of light diffracted into the nth order of the contact print will be calculated. The intensity will be given as a function of the phase shift ϕ occurring in the scene between the two original exposures from which the contact print is made. Other parameters involved are the ratios α and β of the opaque line widths to the fringe spacing. The method of analysis used to derive the formulas is described in Born & Wolf[1].

In Fig. 8-4 one period of the grating is shown. For analysis, it is assumed that the grating is either clear or opaque.

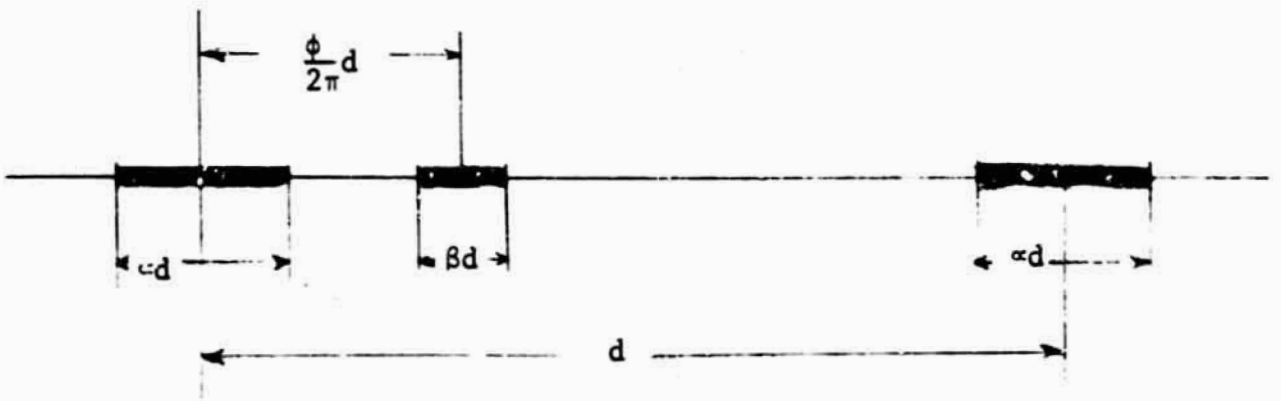

Figure 8-4

[1] M. Born & E. Wolf, Principles of Optics, Macmillan, 1964, See Section 8.6.1.

The period of the grating is d. The portion of the contact print rendered opaque by the first exposure is denoted by the lines of width αd and the portion rendered opaque by the second exposure is denoted by the lines of width βd. The relative displacement of these two sets of fringes is $\frac{\phi}{2\pi} d$ where ϕ is the phase shift occurring in the scene between the two original exposures.

If $\alpha + \beta > 1$, which can be thought of as the case of wide black fringes, then whenever ϕ satisfies

$$1 - \frac{\alpha}{2} - \frac{\beta}{2} \leq \frac{\phi}{2\pi} \leq \frac{\alpha}{2} + \frac{\beta}{2} \quad ,$$

there will be complete obscuration, giving zero intensity and no dependence on ϕ in this range. The avoidance of this condition is why the reversal process of the contact print is required, giving narrow black lines so the above condition does not occur. We henceforth assume that $\alpha + \beta < 1$, so complete obscuration cannot occur.

The analysis divides into three cases:

Case A:

$$0 \leq \frac{\phi}{2\pi} \leq \left| \frac{\alpha}{2} - \frac{\beta}{2} \right| \quad .$$

In this case, the second set of fringes is completely on top of the first set, and thus no ϕ dependence exists. The intensity of light diffracted into the nth order depends only on the wider of the two lines, and is given by

$$I = I_o \frac{1}{\pi^2 n^2} \sin^2 \pi n\gamma \quad ; \qquad \gamma = \max(\alpha,\beta) \quad .$$

Here and in the following, I_o is the incident intensity on the hologram.

Case B:

$$\left| \frac{\alpha}{2} - \frac{\beta}{2} \right| \leq \frac{\phi}{2\pi} \leq \frac{\alpha}{2} + \frac{\beta}{2}$$

In this case, there is partial overlap of the fringes, and the intensity of the nth order diffracted light is given by

$$I = I_o \frac{1}{\pi^2 n^2} \sin^2 \left[n\frac{\pi}{2}(\alpha+\beta) + n\frac{\phi}{2} \right] \quad .$$

Case C:

$$\frac{\alpha}{2} + \frac{\beta}{2} \leq \frac{\phi}{2\pi} \leq \frac{1}{2}$$

In this case, there is no overlap of fringes. The intensity of light diffracted into the nth order is then

$$I = I_o \frac{1}{\pi^2 n^2} \left\{ [\sin\pi n\beta - \sin\pi n\alpha]^2 + [(\sin\pi n\beta + \sin\pi n\alpha)^2 - (\sin\pi n\beta - \sin\pi n\alpha)^2] \cos^2 n\frac{\phi}{2} \right.$$

The intensity function is symmetric in ϕ about the point $\frac{\phi}{2\pi} = \frac{1}{2}$ and about the point $\phi = 0$. Thus the above three cases enable the entire behavior to be described.

An interesting special subcase of Case C is where $\alpha = \beta$. In this subcase the intensity function becomes

$$I = I_o \frac{4}{\pi^2 n^2} \sin^2 \pi n\alpha \cos^2 n\frac{\phi}{2} \quad . \quad (\alpha = \beta) \qquad (3)$$

It is clearly desirable to avoid Case A because of its lack of ϕ dependence, and this may be accomplished simply by making the exposures equal so that $\alpha = \beta$.

Operation with $\alpha = \beta = \frac{1}{2}$ so that Case B applies, is theoretically a possibility, but is not recommended in practice because of its high sensitivity to exposure variations. The physical interpretation of the exposure sensitivity is simply that in this case of partial overlap, a variation in exposure causes a variation in line width, which due to the partial overlap, is equivalent to a shift in the position of the center of the fringe, i.e., to a phase shift.

Case B can never be avoided completely for subjects which have phase variations greater than 2π. Operation with very narrow fringes minimizes the fraction of the hologram for which Case B applies. For subjects which have total phase variations less than 2π, case B can be avoided either by the introduction of a 180° phase shift over the entire scene for one of the exposures or by shifting one of the original exposures by one-half a fringe before contact printing.

The behavior in Case C of no overlap of lines is of primary interest, for this is the most useful domain of operation. From the intensity formula for this case, the most important observation is the dependence of the coefficient of the phase sensitive term, i.e., the coefficient of $\cos^2 n\frac{\phi}{2}$, on α and β. This coefficient becomes zero whenever either α or β takes on a value m/n, where m is an integer. For such values of α or β there is no ϕ dependence of the intensity. In practice, this should not constitute a serious restriction, for by comparing the pictures produced in the various orders one should be able to avoid being misled by aspects of the picture stemming from particular line widths.

Operation in Case C is also favored because lack of exposure control is less harmful than in Case B. By aiming for operation with $\alpha = \beta \simeq \frac{1}{2n}$ the behavior is not particularly sensitive to errors of exposure. From formula (2) one obtains that a factor of two error in exposure changes the line widths by less than 50%, which in turn from formula (3), changes the intensity of the readout beam by only a factor of two, without passing through any zeros.

In interferograms in which the phase ϕ varies more than 2π, the hologram operates in both Cases B and C. The diffraction efficiency of the two cases may not be equal, depending on the particular line widths involved. However, there is no discontinuity at the transition from Case B to C, and the inequality of diffraction efficiency manifests itself only as a first order intensity modulation of the nth order fringes.

8.7 Experimental Results to Date

A number of experimental tests of the two exposure-double contact print process have been carried out with a He-Ne gas laser. The best performance achieved so far is a factor of four, obtained by readout in the fourth order. This is short of our original expectations, and we still hold out hope for further improvement. One of the experimental problems is obtaining narrow line widths with clean edges. The films, of course, do not behave according to the ideal postulated in the analysis, and also such factors as stray light influence the fringe quality. Different emulsions have been tried.

Fig. 8-5 shows the first four orders from a double-exposed contact print. The "subject" in this case was a simple wedge covering the entire scene area, produced by a small rotation of one of the prisms of the arrangement. The increase of phase sensitivity as the order increases is evident. The emulsion used in this case was Kodak 649F. Fig. 8-6a shows a photomicrograph of the fringes of this double exposed contact print. Notice the change in the relative displacement of the fringes from the left side where the lines overlap to the right side where the lines interlace. Notice also the poor quality and broken nature of the fringes, and compare the quality of the fringes to the fringes of the reconstruction (Fig. 8-5). Fig. 8-6b is a photomicrograph of one of the original exposures used in making the contact print. The clear regions are narrow because the exposure used was about 20 times that required for 50-50 fringes.

8.8 Comparison With Conventional Techniques

Until further experimental tests are made, it is not possible to give a true comparison of the new technique to the conventional technique of measuring fringe displacements in Mach-Zehnder interferograms, with accuracies of a fraction of a fringe. However, it is possible to point to three features of the new technique which may be of practical importance.

The first is that each fringe of the final interferogram, viewed in the nth order, results from an average taken over a great many fringes of the contact print. This averaging makes the viewed fringes straighter and more uniform than the individual fringes on the photographic print. This may be seen by comparing the holographic readout interference fringes of Fig. 8-5 to the rather poor quality fringes of the contact print, Fig. 8-6a, which produced them. The extent to which conventional fringe displacement measurements can be made on the holographically reconstructed fringes is unknown at present.

The second feature of the new technique has already been mentioned; it is the ability of the holographic technique to function with imperfect optics and alignment. This property stems from the fact that the holographic process really compares the scene to itself at a later time, thus compensating for any aberrations in the apparatus. Although detailed analysis has not been made, it appears that non-flatness of emulsion supports also does not introduce significant errors.

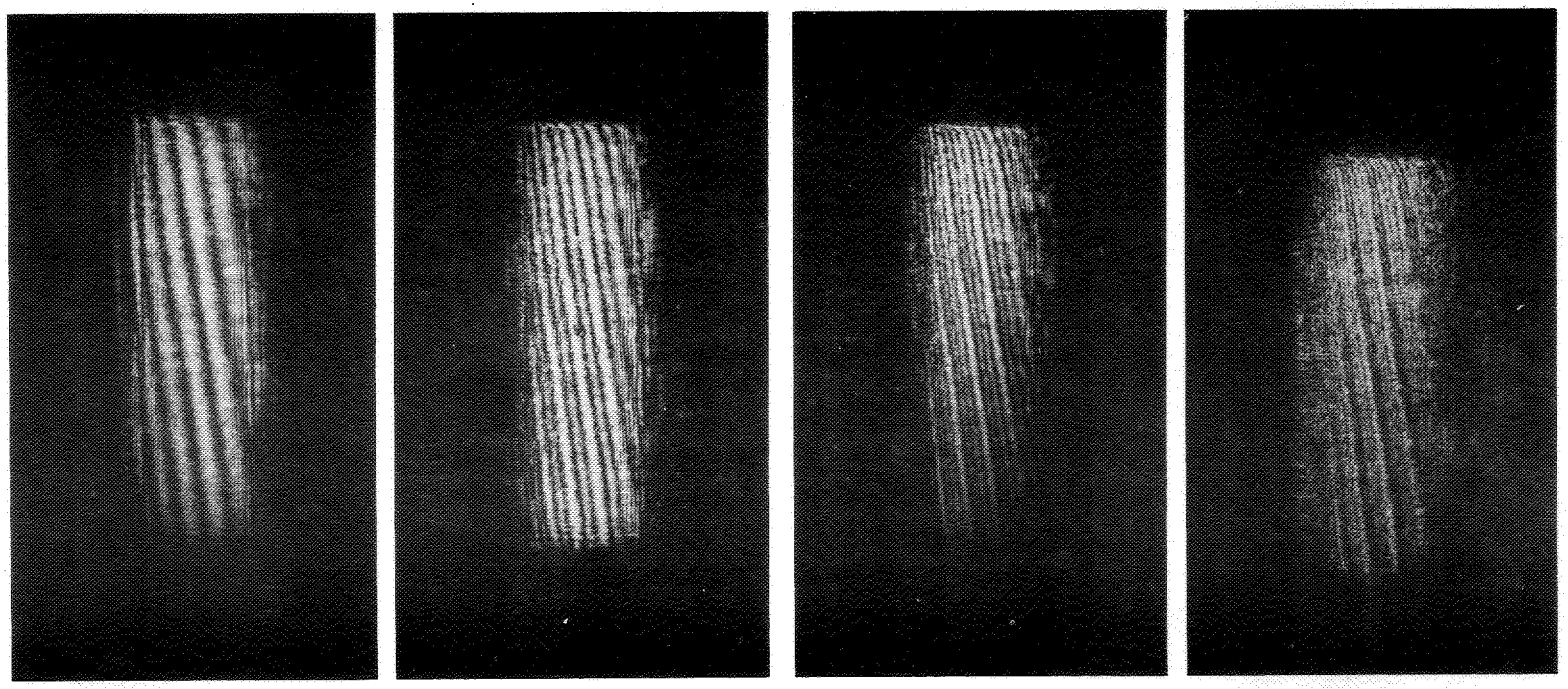

Fig. 8-5. Photos of the holographic reconstruction of the first four orders from a double exposed contact print, made from two separately exposed holograms. The "subject" is a single wedge covering the entire scene, formed by a small rotation of one of the prisms of the assembly. The number of interference fringes is seen to increase with the order, demonstrating the increased phase sensitivity of the high order technique.

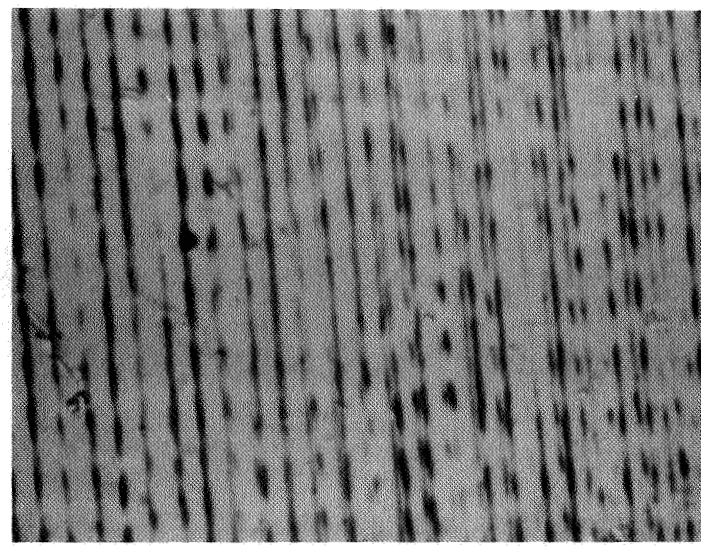

a

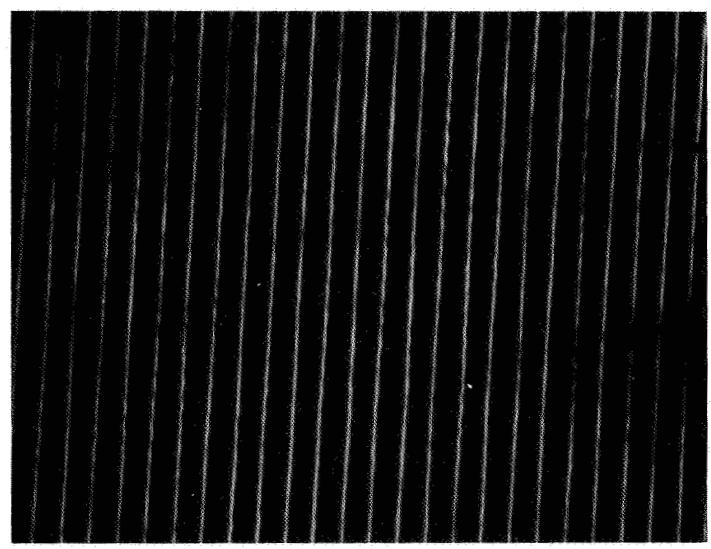

b

Fig. 8-6. a) Photomicrograph of a portion of the contact print used to produce Fig. 6.
b) Photomicrograph of a portion of one of the two original holograms used to produce the contact print shown in (a). The fringe spacing is 40 microns. The emulsion is Kodak 649F.

A third feature which may be of practical importance is simply that the new technique makes small phase shifts evident by visual inspection, avoiding the displacement measuring process involved in the classical approach.

8.9 Further Enhancement of the Intensity of High Orders by Fringe Interpolation

A simple technique for increasing the intensity of light in the high orders consists of interpolating additional lines between the basic lines of the fringe pattern. This is accomplished by displacing the original holograms during the contact printing step. For example, if each original exposure is exposed n times during the contact printing step, with a displacement of one nth the fringe spacing between each exposure, then the resulting contact print will diffract n^2 times as much light at the angle corresponding to the nth order of the original as would a single exposed contact print, provided that the line width is such that overlap of lines does not occur in the multiple exposed contact print.

The principal problem with this technique is that its use tends to change the operation from that of Case C to the less desirable Case B operation.

Fig. 8-7 shows a precision mechanism constructed for producing the required displacements. It has been found to be very effective for increasing the light in high orders from single exposed holograms. However, when applied to the double exposure process, the results so far have not been particularly encouraging, presumably because of the reason mentioned in the preceding paragraph and because of the poor quality of the fringe lines obtained so far.

Fig. 8-8a shows a heavily exposed grating similar to that of Fig. 8-6b, but with coarser fringes. Fig. 8-8b shows a contact print made from this grating in which 10 exposures were made with displacement of 1/10 of a fringe between exposures. The line quality is terrible, but in spite of this, the grating is quite effective in diffracting light to high orders. With one's eye, it is possible to detect light at the angle of the 100th order of the original grating at certain spots on the plate.

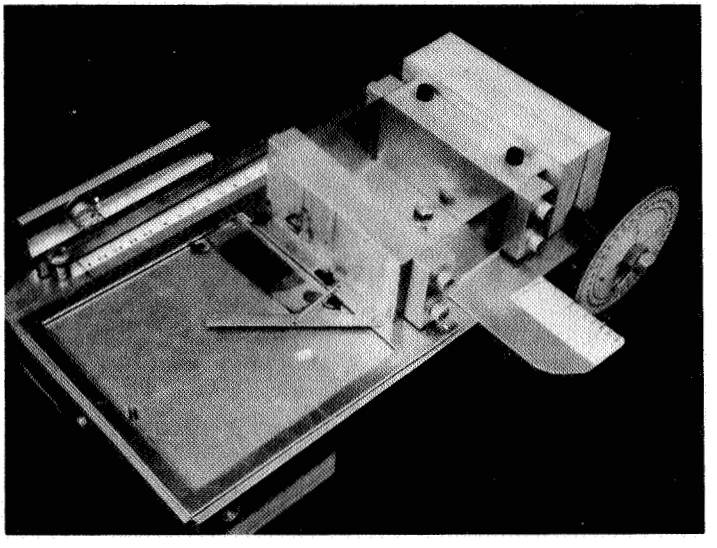

Fig. 8-7. Mechanism used to produce precision-controlled displacements of holograms between exposures of contact printing. This process increases the intensity of the high order diffracted beams.

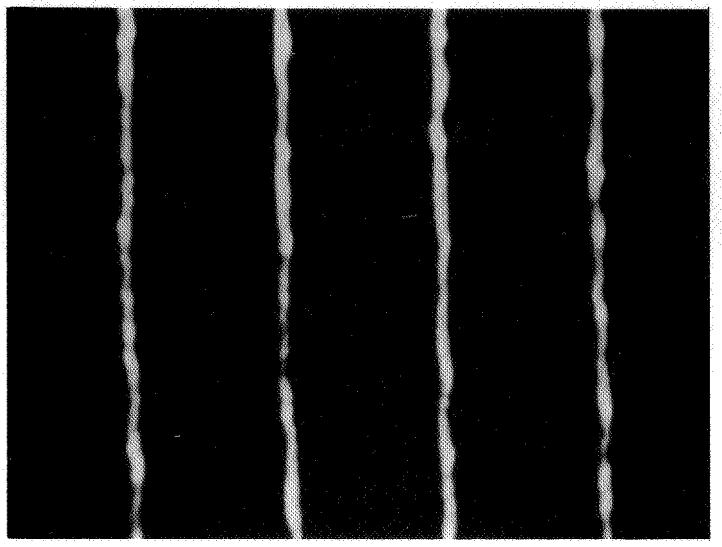

a

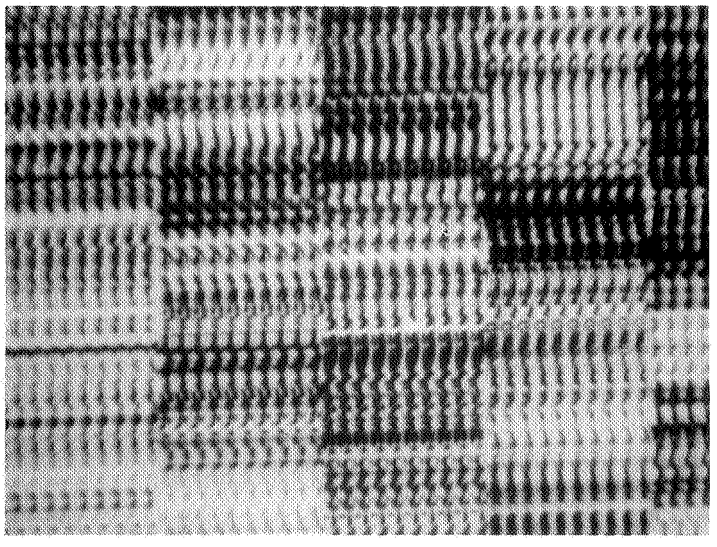

b

Fig. 8-8. a) Photomicrograph of a portion of a heavily exposed grating hologram. The fringe spacing is 330 microns and the clear to opaque ratio is approximately 1 to 10. The emulsion is Kodak Kodalith Pan.

b) Photomicrograph of a 10 exposure contact print made from (a) in which the original hologram was displaced by one tenth the fringe period between each exposure. The emulsion is Kodak 649F. In orders which are a multiple of 10, the diffraction efficiency of (b) is far greater than that of (a).

9.0 MULTIPASS HOLOGRAPHIC INTERFEROMETER

The ability of an interferometer to measure small phase differences in light passing through the subject increases with the number of passes. The additive effect of passing a light beam through the subject many times can result in a measurable phase shift where there otherwise would be none.

The drawback of conventional multipass interferometers is the demand for high quality optics. This arises because phase errors in the optical elements involved in the multiple passage of the light are also multiplied by the number of passes. This need for extremely high quality results in great expense and limits the practical size of the optical elements which can be employed. Since one of the outstanding advantages of holographic interferometry is its tolerance for optical imperfection, it is well suited to multipass interferometry.

Although the multipass holographic interferometer is well suited to either the double-exposure[2] or real-time[3] (single exposure) technique, only the former is discussed in this report.

9.1 Multipass Technique

In order that the subject will be traversed many times by the light, it is placed between two plane mirrors, and the light is introduced at right angles so that it is repeatedly reflected through the subject. If one of the mirrors is partially transparent, a portion of the light will be transmitted through the mirror with each round trip in the subject cavity. The task is then to discriminate between the light beams corresponding to different numbers of round trips.

One method used to select the desired light beam is to introduce a slight angle between the two mirrors so that each beam will emerge with a

slightly different angle. By focusing the emerging beams and placing a narrow slit at the appropriate focal position, the desired beam can be selected and the others rejected.*

Figure 9-1 shows an optical schematic of the apparatus. The basic arrangement is the Twyman-Green modification of the Michelson interferometer, with one arm being used for the subject and the other serving as the reference beam. The incoming laser beam is split into the scene and reference arms by means of a 50-50 beam splitter which is subsequently used to recombine the two beams before they fall on the hologram recording film. The angle between the two beams is kept small so as to permit the use of low resolution film.[5]

The subject beam is expanded with a telescope before it enters the subject cavity. The subject cavity consists of a partially reflecting mirror through which the beam enters and a totally reflecting end mirror. The beam is repeatedly reflected back and forth in the subject cavity, emitting a fraction of its energy through the partial mirror with each round trip in the cavity. The two cavity mirrors are adjusted to have a small angle between them so that the exiting beams are angularly separated. By proper orientation of the cavity with respect to the entering beam, a slit aperture in the focal plane of the telescope objective lens can be used to pass both the entering beam and the exiting beam which has made a designated number of round trips in the subject cavity. Although two separate slits could be used for the entering and exiting beams, it is shown in section 9.3.1 that the single slit results in the minimum amount of lateral beam walking in the subject cavity.

As the intensity of the output subject beam decreases exponentially with the number of cavity traversals, the system makes less efficient use of the light and becomes more susceptible to the problem of stray reflections. In addition, subject resolution decreases and cumulative phase aberrations in the

---

* In principle, it is possible to eliminate the selecting aperture and record all of the emerging beams on the hologram. Because they are angularly separated, the desired beam can be selected upon reconstruction, permitting the operator to postpone the decision as to how many passes he wishes to observe. In practice, the recording of many images decreases the signal-to-noise ratio of each, and the problem is compounded for a large number of passes because of the weak beam intensity.

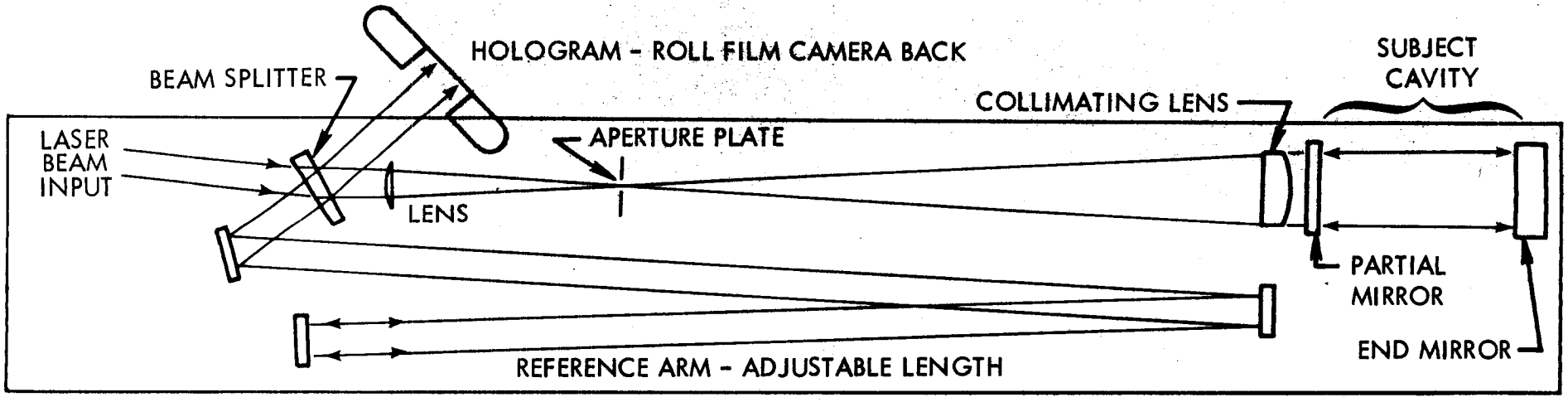

Fig. 9-1. Optical schematic of multiple-pass holographic interferometer using the basic Twyman-Green arrangement. The beam in the subject arm is enlarged using an expansion telescope consisting of two positive lenses. The subject beam is made to pass many times through the subject by the presence of a partially reflecting mirror in the arm. With a slight angle between the partial mirror and end mirror, the slit aperture in the focal plane of the collimating lens selects the beam having the desired number of passes through the subject.

beam due to phase errors in the optical elements and in the subject increase, ultimately limiting the number of round trips for which the technique is useful. The system is most compatible and useful with subjects having very small variations in optical thickness, such as low pressure gas phenomena.

9.2 Light Efficiency

Because only a fraction of the light emerges from the subject cavity after having passed through the subject a specified number of times, the efficiency of the light in the subject beam is an important factor. If there are N round trips in the subject cavity, the subject light passes through the subject 2N times, and the phase sensitivity of the interferometer is increased 2N times. Let the reflectivity of the partial mirror be r, and assume that it is non-absorbing. Thus its transmittance is 1 - r. If the end mirror is assumed to be 100% reflecting, and absorption by the subject is neglected, the fractional efficiency of the subject beam after the Nth round trip in the subject cavity is

$$S_N = (1 - r)^2 \, r^{N-1}$$

Setting the derivative with respect to r equal to zero, the reflectivity which maximizes the energy S_N is

$$r_N = \frac{N - 1}{N + 1} \quad ,$$

and the value of S_N with the optimum reflectivity is

$$S_{N\ opt} = \left(\frac{2}{N + 1}\right)^2 \left(\frac{N - 1}{N + 1}\right)^{N-1}$$

As N becomes large, the fractional efficiency tends toward the quantity

$$S_{N\ opt} = \frac{4}{e^2(N^2-1)} \approx \frac{.54}{N^2-1} \quad .$$

If the end mirror is not perfectly reflecting, as is often the case, the optimization procedure is not changed, but the fractional efficiency is decreased by the end mirror reflectivity raised to the Nth power. Fig. 9-2 shows a plot of the optimum fractional efficiency (assuming a perfect end mirror) as a function of the number of cavity round trips N.

Although a desirable feature of the holographic interferogram is that the fringe contrast depends only on the ratio of the reconstructed light intensity to the scattered light intensity (assuming equal exposures), and only indirectly on the contrast of the hologram itself, as a practical matter it is desirable to have the hologram of as high contrast as possible. To achieve high contrast, the reference arm of the interferometer is attenuated, resulting in a total light efficiency proportional to the efficiency of the subject arm.

9.3 Image Resolution

As the number of round trips in the subject cavity is increased, there is a corresponding decrease in the image resolution. This can result from beam "walking" in the subject cavity, diffraction effects stemming from the limited size of the angle-selecting aperture, and multiple images resulting from repeated reflection by the cavity mirrors. In the following sections, these effects will be examined separately and jointly.

9.3.1 Beam Walking

When an angle-selecting aperture is placed at the focal plane of the collimating lens to discriminate in favor of the beam having a specified number of passes in the subject cavity, a small angle is introduced between the two mirrors constituting the cavity so that with each round trip the beams will emerge angularly separated.* However, in addition to producing an angular

* It is possible to postpone the insertion of the angle-selecting aperture until the reconstruction of the hologram, and in principle to defer until that time the selection of the angle, and hence the value of N, to be viewed. The simultaneous recording of many beams of widely varying intensities may pose practical difficulties.

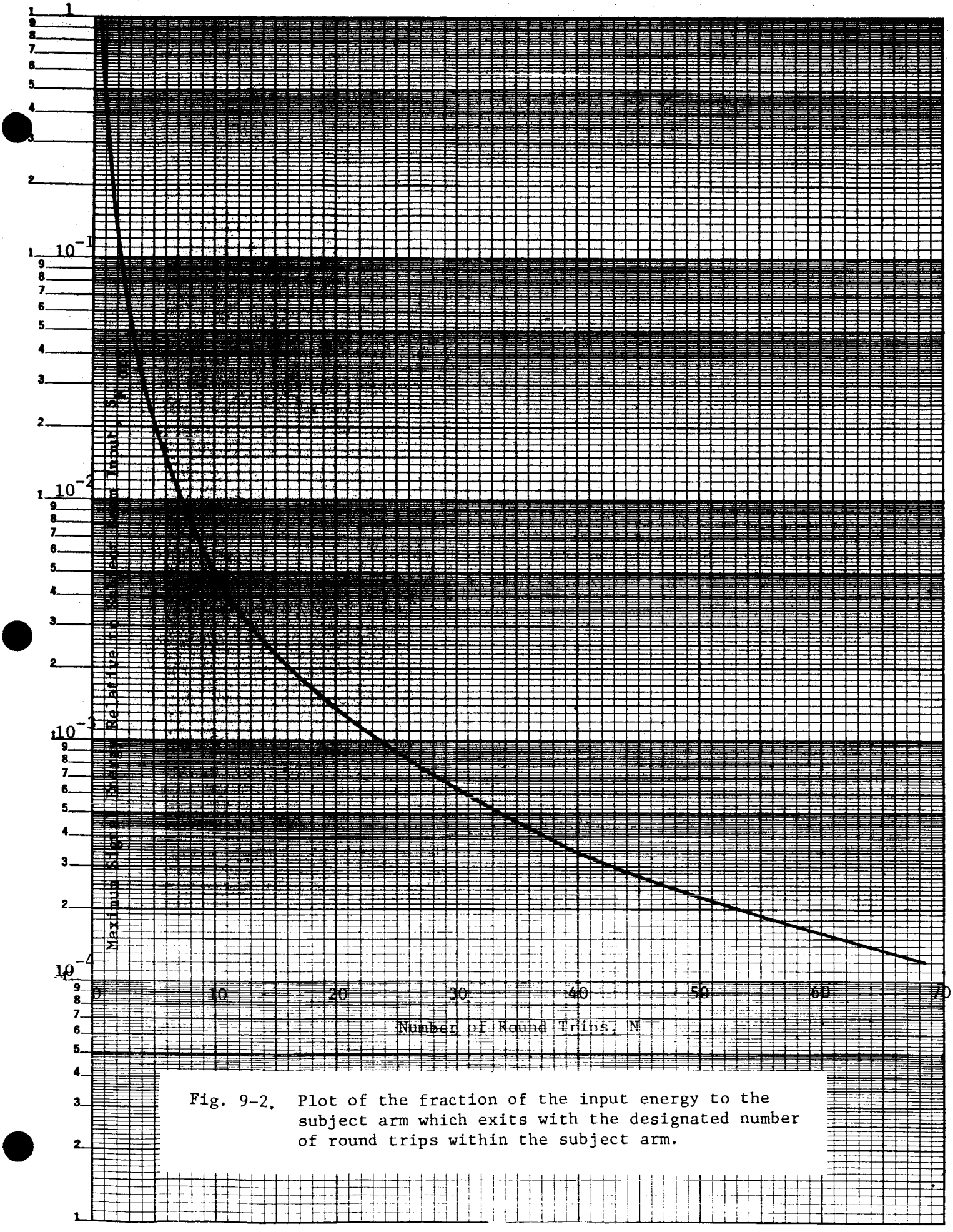

Fig. 9-2. Plot of the fraction of the input energy to the subject arm which exits with the designated number of round trips within the subject arm.

separation of the beams, there is also a lateral walking of the beam parallel to the plane of the cavity angle. This lateral walking causes a lateral smearing of each point on the subject and reduces the image resolution in the lateral direction.

Using geometrical optics, this effect can be studied. Fig. 9-3 shows the subject cavity and the path of a ray making its entrance into the cavity. The partial mirror is on the right and the end mirror (100% reflecting) is on the left. The coordinate system has been chosen such that the partial mirror is vertical and all angles are taken to be positive in the counter-clockwise direction.

Let α_n denote the angle with the horizon of a ray making its nth traversal of the cavity and ψ denote the angle of the end mirror. Thus, the nth ray impinging on the end mirror (n odd) is reflected with an angle

$$\alpha_{n+1} = -\alpha_n + 2\psi \quad , \quad n \text{ odd}$$

The nth ray impinging on the partial mirror (n even) is reflected with an angle

$$\alpha_{n+1} = -\alpha_n \quad , \quad n \text{ even}$$

These two equations give a recursion formula for computing the angle of the nth ray, in terms of the entrance ray angle α_1 and the end mirror angle ψ.

$$\alpha_n = \begin{cases} \alpha_1 - (n-1)\psi & , \ n \text{ odd} \\ -\alpha_1 + n\psi & , \ n \text{ even} \end{cases} \tag{1}$$

Let δ_n denote the displacement of the ray due to its nth traversal of the cavity measured from its point of intersection of the mirrors. Using Eq. (1) and the small angle approximation, the displacement can be written,

$$\delta_n = \begin{cases} -\alpha_n D = \left[-\alpha_1 + (n-1)\psi\right] D & , \ n \text{ odd} \\ \alpha_n D = \left[-\alpha_1 + n\psi\right] D & , \ n \text{ even} \end{cases}$$

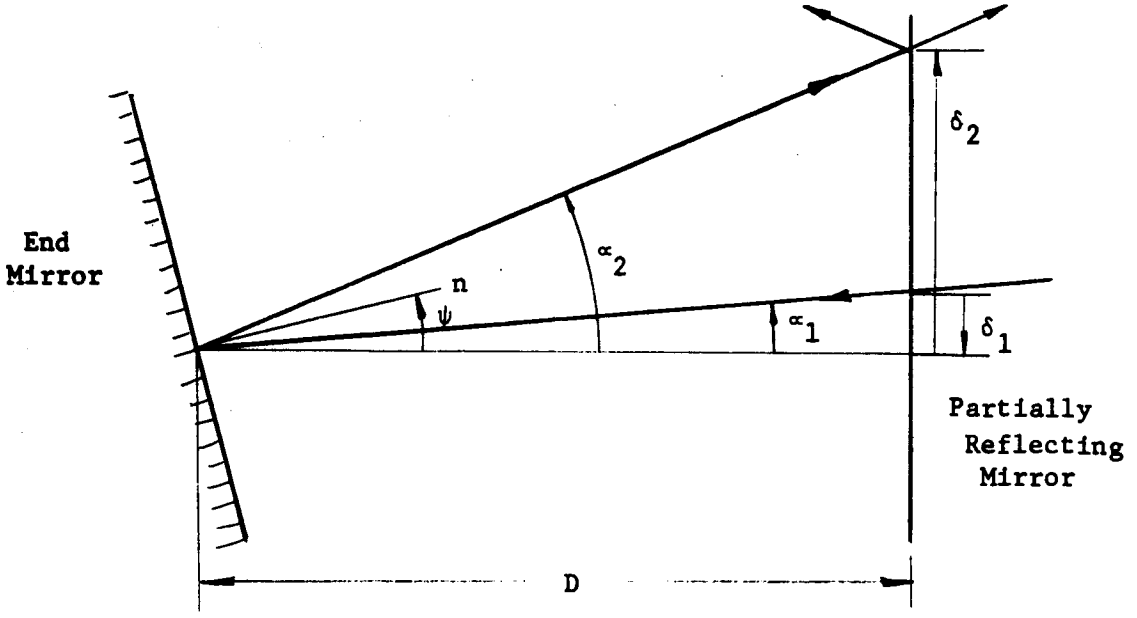

Fig. 9-3. Subject cavity geometry with angles greatly exaggerated.

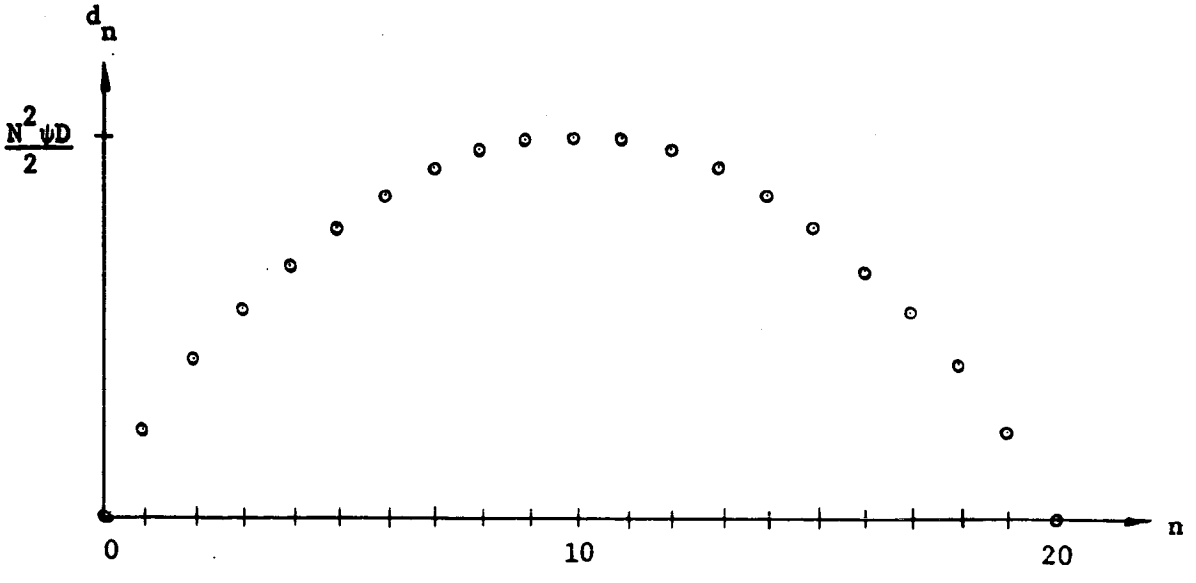

Fig. 9-4. Graph of cumulative beam displacement as a function of the number of cavity traversals for $\alpha_1 = N\psi$.

The cumulative displacement d_n can be written,

$$d_n = \sum_{i=1}^{n} \delta_i = \sum_{i\ odd}^{n} \delta_n + \sum_{i\ even}^{n} \delta_n$$

$$= \sum_{i\ odd}^{n} \left[-\alpha_1 + (n-1)\psi\right] D + \sum_{i\ even}^{n} \left[-\alpha_1 + n\psi\right] D$$

$$= \sum_{i=1}^{n} \left[-\alpha_1 + n\psi\right] D + \sum_{i\ odd}^{n} (-\psi)\ D$$

The case of interest is where n is even, that is, where the ray makes an integral number of round trips in the cavity. For this case d_n can be written

$$d_n = -\alpha_1 nD + \frac{n(n+1)\psi D}{2} - \frac{n}{2}\psi D$$

$$= (-\alpha_1 + \frac{n}{2}\psi)nD \qquad (2)$$

Thus the displacement d_n follows a parabolic law. With reference to Fig. 9-4, it is intuitively clear that the minimum beam walking range is obtained when the cumulative displacement is zero, obtained by setting $\alpha_1 = \frac{n}{2}\psi$.* In this case, the beam walks in one direction, reverses direction and walks back to the starting point where it leaves the cavity as the useful output. Fig. 9-4 shows the beam walk as a function of n for this case. Because the entering and exiting subject beams are parallel to one another, the angle-selecting aperture consists of a single slit. The maximum ray excursion from the input position, determining the maximum image smear, occurs as the ray has made half of its total cavity traversals. The maximum excursion is obtained by substituting n/2 for n and letting $\alpha_1 = \frac{n}{2}\psi$ in Eq. (2), giving a maximum smear due to beam walking or,

$$r_{bw} = (-\frac{n}{2}\psi + \frac{n}{4}\psi)\frac{n}{2}D = -\frac{n^2\psi}{8} D \qquad (3)$$

---

* The close angular proximity of the strongest cavity output (first round trip) to the desired cavity output poses a possible crosstalk problem that may require greater than the minimum angular beam separation.

Letting N denote the number of round trips of the subject beam so that $n = 2N$, Eq. 3 can be written

$$r_{bw} = \frac{N^2 \psi D}{2} \tag{4}$$

Reference to Fig. 9-4 shows that the effective smearing is less than the extreme smearing due to the concentration of ray displacements about the maximum d_n. However, we shall make no allowance for this in the following.

From Eq. (1) we see that the angular separation of the return beams is 2ψ. The maximum slit width s at the focal plane of the objective lens having a focal length f is given by

$$s = 2\psi f \quad . \tag{5}$$

Using Eq. (5), Eq. (4) can be written

$$r_{bw} = \frac{N^2 sD}{4f} \tag{6}$$

9.3.2 Multiple Images

A second effect which reduces the resolution of the multiple pass interferometer is the presence of multiple images due to the successive reflection of the subject in the reflecting cavity. These images are spaced by the cavity spacing D from one another as shown in Fig. 9-5.

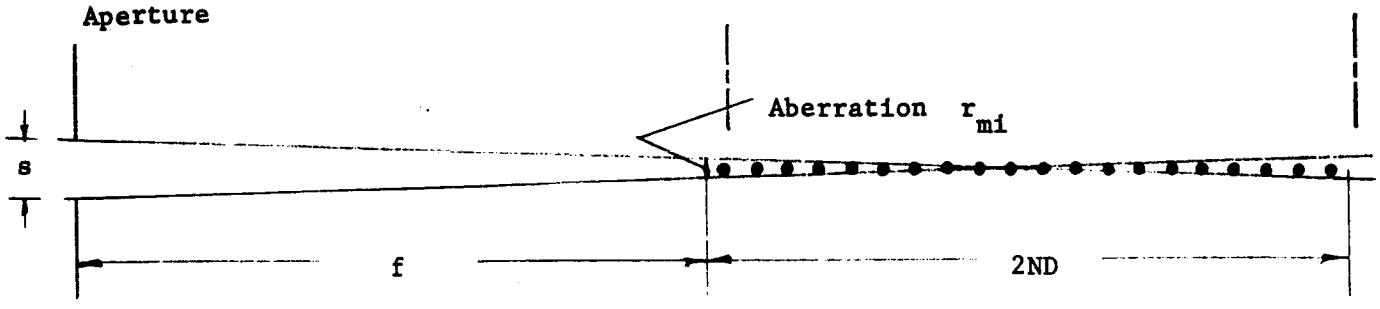

Fig. 9-5. Multiple images.

To minimize the out-of-focus effect, one focuses on the middle image. The geometrical spreading of the extreme images can be written

$$r_{mi} = \frac{sND}{f + ND} \tag{7}$$

9.3.3 Diffraction-Limited Image Resolution

A third effect limiting the image resolution is the diffraction effect associated with the angle-selecting aperture. A narrow slit aperture, desirable in order to minimize the effect of beam walking, acts as a one-dimensional, low-pass, spatial filter for the subject and thereby limits the image resolution. Assuming no aberrations, and using the Rayleigh criterion, the angular resolving power of a slit of width s is given as $\frac{\lambda}{s}$. The distance from the slit to the midpoint of the multiplicity of images is approximately f + ND, and the resulting image resolution is,

$$r_d = \frac{\lambda}{s}(f + ND) \quad . \tag{8}$$

9.3.4 Optimum Image Resolution

We have seen that contributions to image smear can come from beam walking, the existence of multiple images, and diffraction effects. For the case where an angle-selecting aperture is employed, all of these effects must be considered. The problem is to choose system design parameters such that the total image smear is minimized. While the exact solution of the problem is complicated, it is possible to obtain an approximate solution by simple considerations.

If we assume that the total image smear is the sum of its contributions as given by Eq. (6), (7), and (8), the total smear can be written,

$$r = r_{bw} + r_{mi} + r_d = \frac{N^2 sD}{4f} + \frac{NsD}{f+ND} + \frac{\lambda}{s}(f + ND) \quad .$$

Setting the derivative of r with respect to s equal to zero, we can solve for the value of s^2 which minimizes the image spread.

$$\frac{\partial r}{\partial s} = \frac{N^2 D}{4f} + \frac{ND}{f+ND} - \frac{\lambda}{s^2}(f + ND) = 0 \quad ,$$

$$s^2 = \frac{\lambda(f + ND)}{\frac{N^2 D}{4f} + \frac{ND}{f+ND}} \quad . \tag{9}$$

The two terms in the denominator of Eq. (9) are due to the contributions of beam walking and multiple images. If one of these terms is larger than the other, it is the dominant effect and the smaller term may be ignored. Thus, in general, the optimum slit width is either a trade-off between beam walking and diffraction effects, or between multiple images and diffraction effects. Comparing the two denominator terms of Eq. (9), one can see that if the inequality,

$$\frac{ND}{f} > \frac{4}{N} - 1 \tag{10}$$

is satisfied, the beam walking term is dominant and for practical purposes the effect of multiple images can be neglected. Since the inequality (10) is satisfied for $N \geq 4$, we can safely ignore the multiple image term for many cases of interest. Neglecting the multiple image term, the optimum slit width is

$$s = \frac{2}{N}\sqrt{\frac{\lambda f(f+ND)}{D}} \quad , \tag{11}$$

and the total image smear is,

$$r = N\sqrt{\frac{\lambda D(f+ND)}{f}} \quad . \tag{12}$$

Example Calculation

In order to assess the performance of the system under construction, we shall assume some typical design values and determine the slit width and image smear. Taking the following values,

$$N = 5 \text{ (10 passes)}$$
$$f = 500 \text{ mm}$$
$$D = 50 \text{ mm}$$
$$\lambda = .63 \times 10^{-3} \text{mm}$$

the optimum slit width is .9 mm and the image smear is 1.1 mm.

9.3.5 Optimum Image Resolution Without Beam Walking

If other means are used to separate out the desired cavity beam, then the cavity mirrors can be made parallel and the contribution of beam walking to image smear becomes zero. One such method for providing beam separation is to rapidly shutter the subject beam by a Kerr or Pockels cell to allow only the desired beams to pass. Because the subject beam is nominally collimated, the beam diameter can be reduced to a very small value requiring only a small shutter.

In addition to minimizing power requirements and cost, a small shutter minimizes the problem of random phase disturbances, and any random disturbances that do occur are multiplied only by a factor of two since the shutter lies outside the subject cavity.

Another attractive possibility for electro-optical shuttering is to use an electronically-gated image tube in place of the hologram recording film. Diode image tubes with resolution of 50 lines per millimeter and shutter duration of 5 nanoseconds have been developed, and should prove quite satisfactory for the low spatial frequencies encountered in the narrow angle hologram systems which have been discussed. Image distortion is not of great importance. In this case the hologram would be recorded by a camera focused on the output of the image tube.

A second method for selecting the desired cavity beam is to utilize a laser with a controlled coherence length (or pulse length) and make use of the fact that the hologram pattern is formed only by those components of the reference and subject beam which are coherent with one another. By suitably adjusting the reference arm delay, a specified number of cavity round trips can be caused to form a hologram. The remaining pulses, although they strike the film, do not coherently interfere and serve only to fog the film. Depending on the graininess of the film, the ratio of the fog level to the useful holographic exposure can be rather high.

For the case where beam walking is not significant, the optimum aperture width is given from Eq. (9) as,

$$s = (f + ND)\sqrt{\frac{\lambda}{ND}}$$

and the total image smear is,

$$r = 2\sqrt{ND\lambda} \tag{13}$$

Example Calculation

Using the values of the previous 10 pass example, the optimum aperture width for the case of no beam walking is 2.6 mm, and the corresponding image smear is .8 mm.

9.4 Limitations of Multiple-Pass Interferometry

As can be seen from Eq. (12) and (13), a problem of the multiple-pass interferometer is the loss of image resolution with large numbers of cavity traversals and large cavity separation. Because the image blur increases as N for the angle-selecting system (keeping f = ND), but only as $N^{1/2}$ for the case when beam walking is negligible, the latter case is more suitable for a very large N.

Even though the laser pulse can be negligibly short, the total delay time in the cavity, equal to 2ND/c, can be quite appreciable. When the interferometer is used with very high speed subjects, the resulting blur can be significant. For example, a projectile moving 10^4 meters per second through a cavity with separation of 1.5 meters and 100 round trips will travel 1 centimeter during the total cavity delay time. However, if the subject is moving in only one direction, the beam

can be caused to walk to match the subject velocity so that the effect of subject motion can be reduced. If the mirrors are parallel, the matching can in principle be perfect for a constant velocity subject. If the mirrors are not parallel, the matching is only approximate (straight line approximation to the parabola).

9.5 Composite System

When coherence matching alone is used for beam separation, the brightness of the hologram reconstruction decreases with increasing N. This effect either restricts one to fine grain recording materials or a small value for N. When time gating alone is used, it is necessary to insure that the shutter duration is less than the round trip cavity transit time, placing high demands on the electronic driving circuitry when a short cavity is used.

An attractive solution to the problems of using one or another selection scheme alone, is to use a combination of schemes. For example, if coherence matching is used to provide a "fine" selection of desired cavity pulse, the simultaneous use of either optical shuttering or angle selection for "coarse" selection can eliminate all but a few of the cavity beams, thereby greatly reducing the hologram fog level. Because the optical shutter or angle-selecting aperture need not select only a single cavity beam, as they would if used alone, the shutter pulse width can be relatively long or the selecting aperture wide, thereby greatly reducing problems with high speed electronics or beam walking.

9.6 Experimental Results

Using the arrangement shown in Fig. 9-1 and 9-6, the soundness of the multipass holographic interferometer was verified. A Spectra-Physics model 131 He-Ne gas laser with a rated output of 0.5 milliwatts was used as the illumination source. Its output was electromechanically shuttered, spatially filtered and collimated into a two-inch diameter beam. To achieve greater amplitude uniformity, only the central portion 0.875 inches in diameter was used. This beam was enlarged three times by the subject beam telescope before entering the subject cavity.

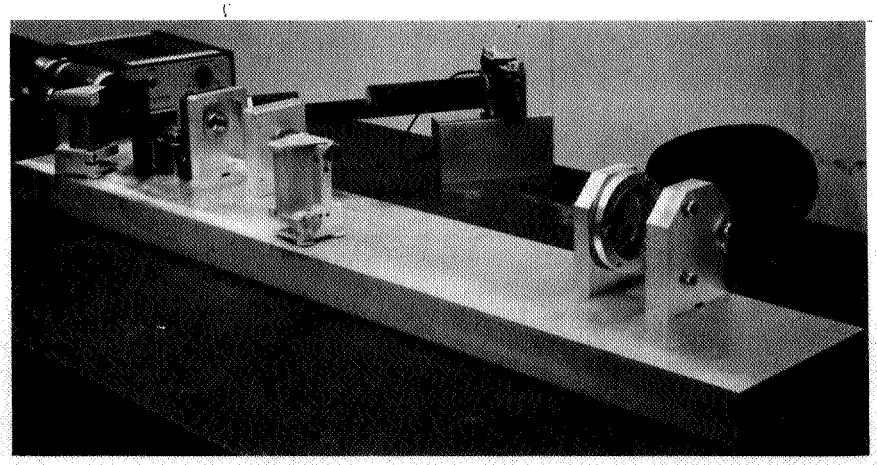

Fig. 9-6. Photograph of the multipass, holographic interferometer.

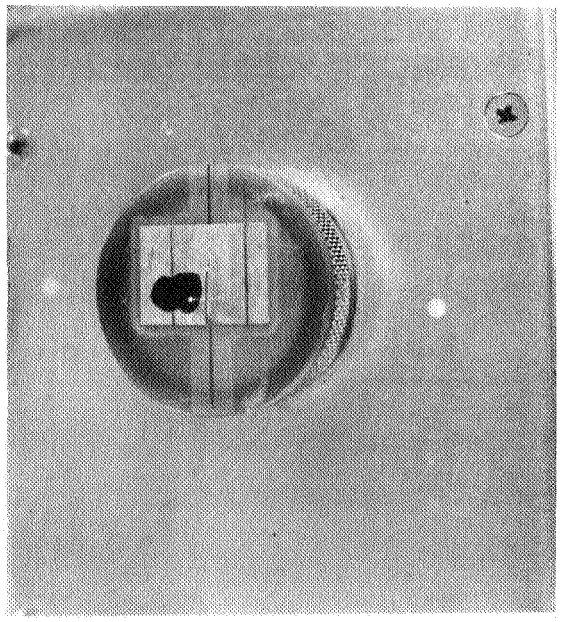

Fig. 9-7. Photograph of the angle-selecting aperture at the focus of the beam expansion telescope. With increasing number of round trips, the focused spot moves to the right, with the brightest spot on the left corresponding to zero round trips (direct reflection from the partial mirror). The dab of black paint was found necessary to reduce the "cat's eye" reflection from this first spot. The two very widely spaced reflections are from the front (antireflection coated) surface of the partial mirror and their large spacing is due to the 1° wedge of the partial mirror.

The subject cavity with a 2-inch separation consisted of a dielectrically coated wedge (1° wedge angle) with a reflectivity of 82% (optimum for 20 passes) and an aluminized end mirror. Both of these elements were specified to have a flatness of 1 wavelength which turned out was sufficient to permit good operation for 10 passes (N = 5) or less.

Although it was not necessary to match the intensities of the subject and reference beams, the best holograms were obtained when this condition was approximately satisfied. A neutral density filter with optical density 1.0 was placed in the reference arm giving a total attenuation of 100 times (two passes) and resulted in reference and subject beams of approximately equal intensities for ten pass operation. Using Plus-X film to record the holograms, a total exposure time of 1/25 second (two exposures) gave good results.

With zero angle between the subject and reference beams, a conventional interferogram was recorded, showing the phase aberrations of the system for 20 passes (see Fig. 9-8). The aberrations are attributable almost entirely to phase errors in the components of the subject cavity.

A series of holographic interferograms were made of a quartz flat, 1 x 1-1/4 x 1/8 inch, with values of N ranging from 1 through 10 (2 through 20 passes). The first six of these are shown in Fig. 9-9. Because of the severity of the aberrations of the system and the weakness of the subject beam in relation to spurious reflections in the system, operation of greater than 10 passes was not judged satisfactory.

Although the input lens to the subject beam telescope was antireflection coated, it still reflected enough (approximately 1%) of the input light to cause trouble. The bright spot in the center of Fig. 9-8 is due to this reflection. Although this could be partially eliminated by spatially filtering the reconstructed beam, it was found more satisfactory to spatially filter the light before making the hologram recording. A spatial filter, shown in Fig. 9-10 was attached directly to the camera body holding the recording film. The filter consisted of a lens to bring the input beams to a focus, a small aperture to permit only the subject and reference beams to pass through, and a second lens near the film to recollimate the beams.

Fig. 9-8. An interferogram of the holographic system for 20 passes showing the phase aberrations of the system. These aberrations do not affect the accuracy of the holographic interferograms, but do limit the maximum number of passes. The central bright spot is due to a spurious reflection.

2 passes

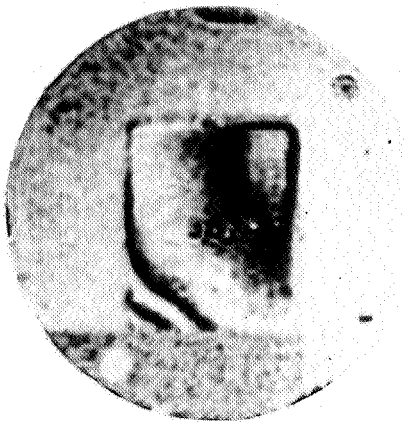

4 passes

6 passes

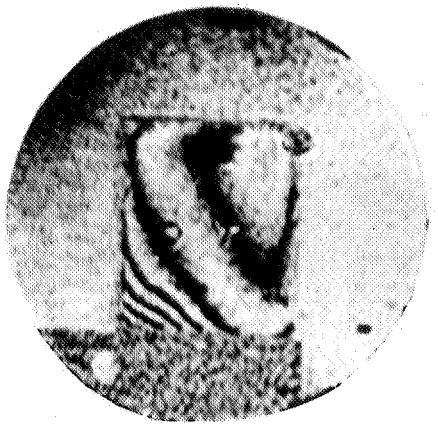

8 passes

10 passes

12 passes

Fig. 9-9. Holographic interferograms of a high quality quartz plate. Background fringes are due to air currents.

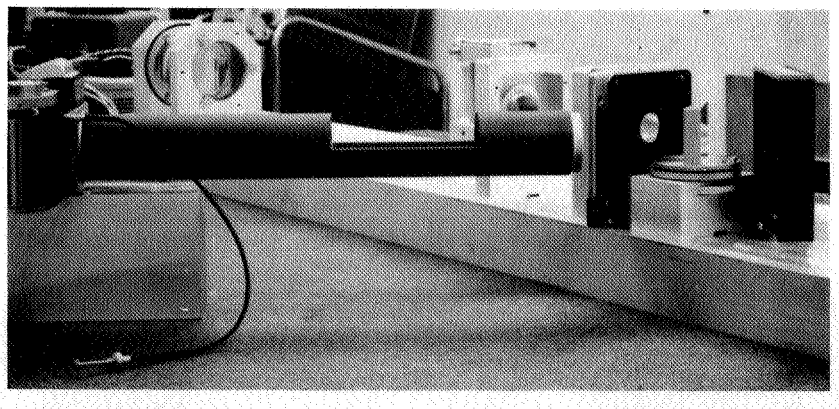

Fig. 9-10. Photograph of the spatial filter attached to the camera body holding the hologram recording film. Two one-inch diameter collimating lenses are mounted in each end of the tube with their focal planes at the center of the tube where a small aperture is located. The tube is cut away to facilitate the positioning of the aperture.

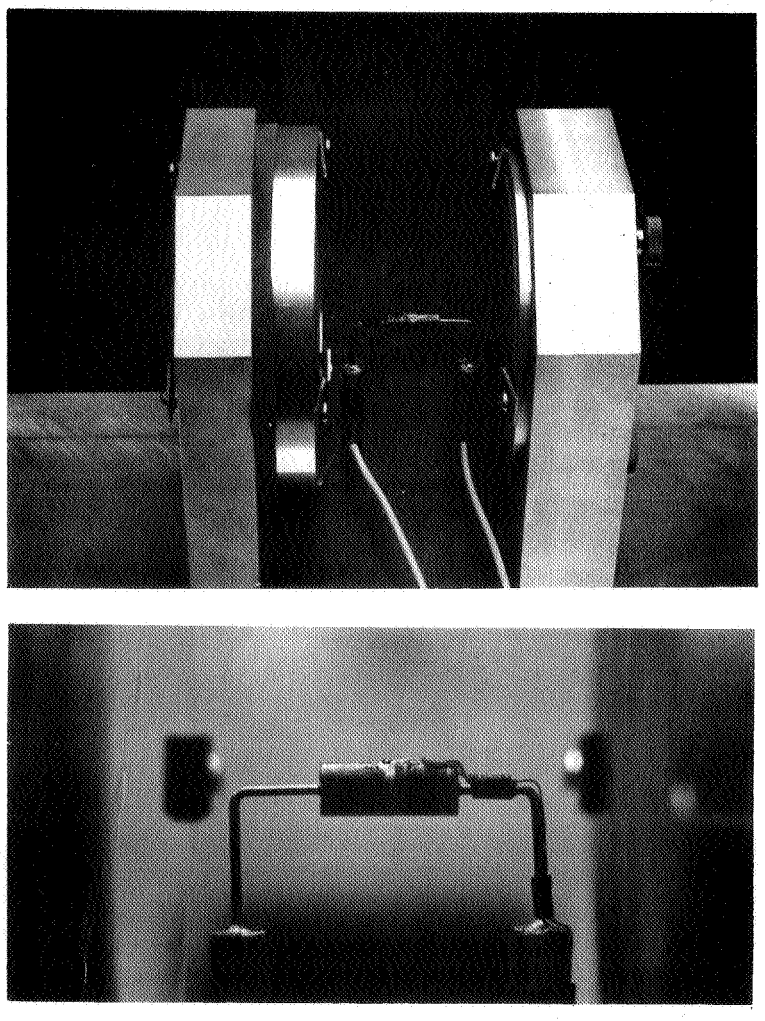

Fig. 9-11. Photograph of the subject cavity and a 1 watt carbon resistor being used as the subject. The resistor is electrically heated and its temperature is monitored by an attached thermocouple.

With the spatial filter installed on the camera body, another series of holograms were made of a 1 watt carbon resistor (5.7 x 14.6 mm) viewed end on, as shown in Fig. 9-11. A current was passed through the resistor, and its temperature rise monitored by an attached thermocouple. The resulting interferograms are seen in Fig. 9-12. The finite fringe interferograms were made by slightly changing the angle of the reference beam between exposures.

Conclusions

The results of the multipass experiments were very encouraging. Good holograms were obtained with 10 passes, and subject resolution appeared to be quite good. Although disappointed that the system aberrations limited operation to 10 passes, it is felt that operation for greater sensitivity should be no great problem. Background fringes due to uncontrolled air currents can be eliminated by better shielding of the apparatus, and the deleterious effects of spurious reflections can be reduced by the use of double antireflection coatings and the more careful construction of the spatial filter apertures.

A most fruitful area for further work is the combination of angle selecting and coherence matching techniques.

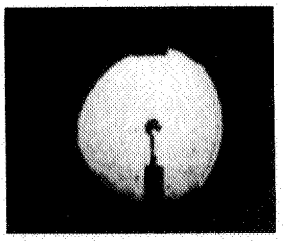

(a) 0° rise

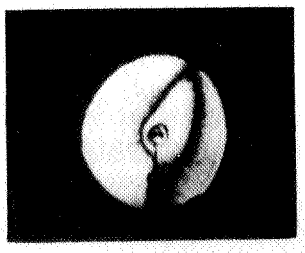

(b) 7.5° C

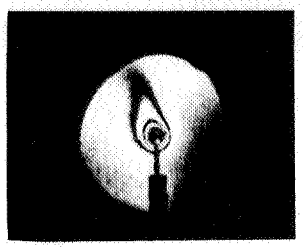

(c) 16.3° C

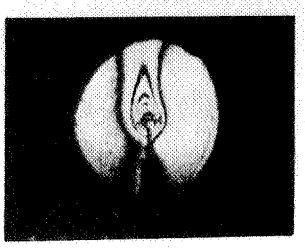

(d) 30° C

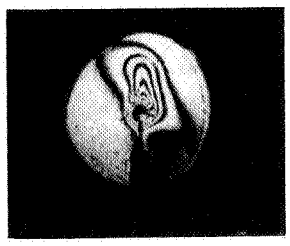

(e) 45° C

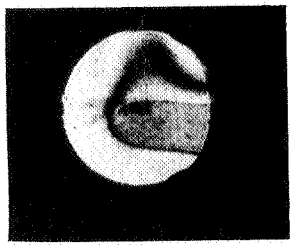

(f) ?° C

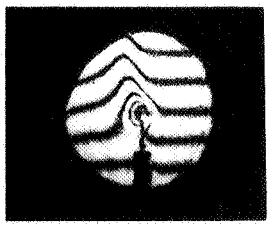

(g) 16.3° C

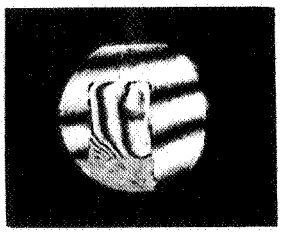

(h)

Fig. 9-12. Holographic interferograms with 10 passes (N = 5). (a) - (e) A one-watt carbon resistor (viewed end on) was electrically heated and its temperature rise measured by an attached thermocouple. (f) A human finger used as the subject. (g), (h) Finite fringe interferograms of the resistor and quartz plate.

10.0 MICHELSON HOLOGRAPHIC INTERFEROMETER FOR USE WITH A PULSED RUBY LASER

Using the basic Michelson configuration, a simple holographic interferometer was constructed for use with a Q-switched ruby laser and Mach 3 projectiles. This represents an attempt to use techniques for increased phase sensitivity in a realistic situation. Tests of the high order technique are not yet completed as of the time of writing, but results with the first order reconstruction demonstrate the ease with which interferograms can be made and how the advantages of holographic interferometry can be exploited.

The test setup is shown in Fig. 10-1. The beam from the Q-switched ruby laser oscillator is first allowed to travel approximately 50 feet, and then only the central portion of it is used in order to eliminate many of the off-axis rays and to improve its uniformity. The laser light is then expanded into a 5" diameter collimated beam by means of lenses L_1 and L_2. The collimated beam is split by the wedge beam splitter into a reference arm and a scene arm, and then subsequently recombined with an angle of about 1° between them and directed toward the hologram.

In order to reject stray light, principally arising from second surface reflections of the beam splitter, a spatial filter identical in principle to that used with the multipass interferometer (see Fig. 9-10) was constructed using lenses L_3, L_4 and a small aperture. Lens L_3 focuses the desired light through the aperture, after which it is recollimated by Lens L_4 before falling on the hologram. Although the second face of the beam splitter was anti-reflection coated, the unwanted light was sufficient, without the spatial filter, to spoil the high order process.

Fig. 10-2 shows the wooden box which was used to mount the optical components of the interferometer. The lenses are 5" diameter, 24" focal length achromats capable of focusing a collimated beam of light to within a one-tenth millimeter diameter circle. The front surface aluminized mirrors were made of selected plate glass. The thin wedge beam splitter, the element contributing the greatest amount of phase aberrations, was also made from selected plate glass, ground and repolished on one side. One face was coated for 20%

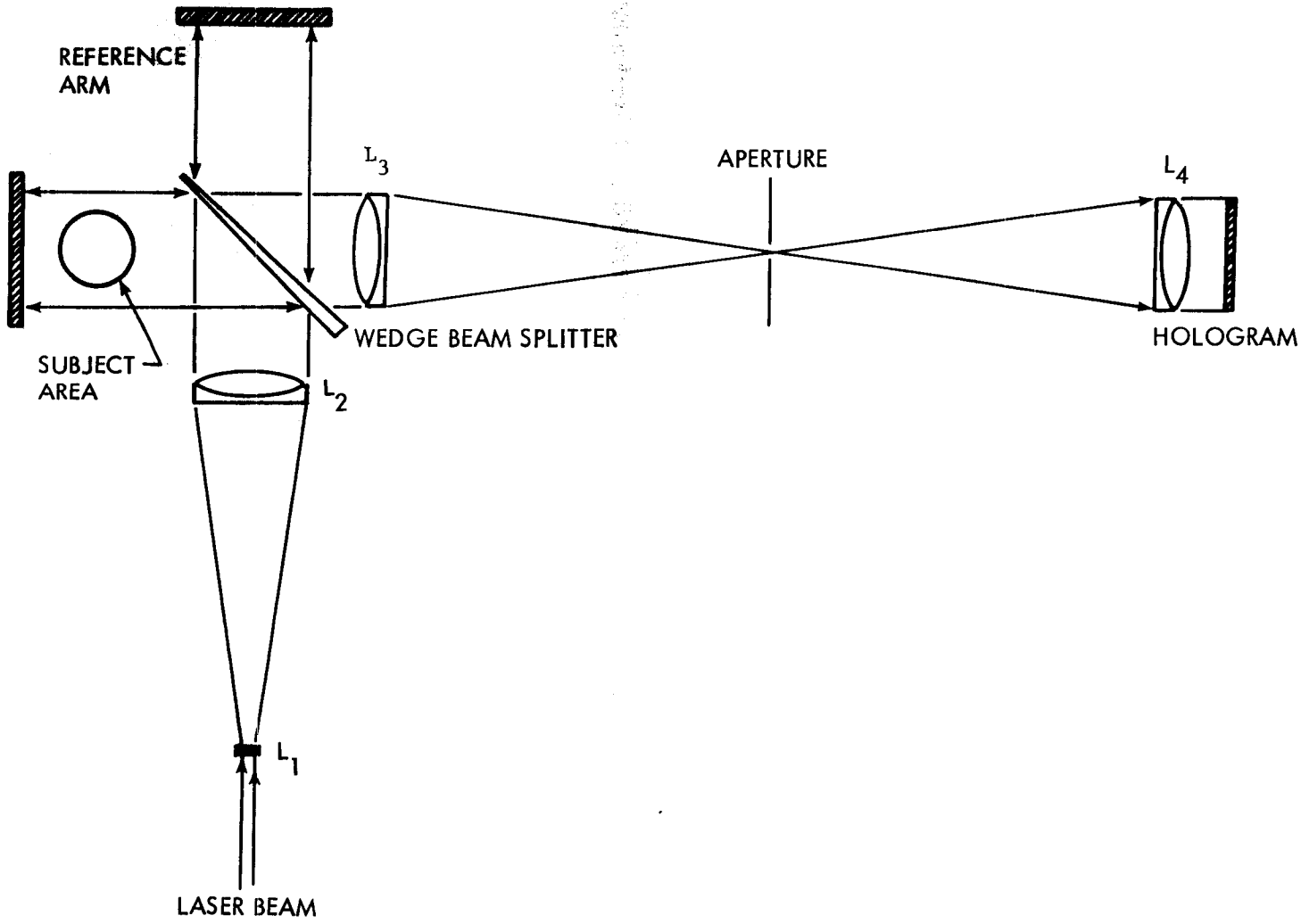

Fig. 10-1. Optical schematic of the Michelson holographic interferometer used with the pulsed ruby laser. Lenses L_3, L_4, and the aperture are used to spatially filter the light to remove spurious reflections.

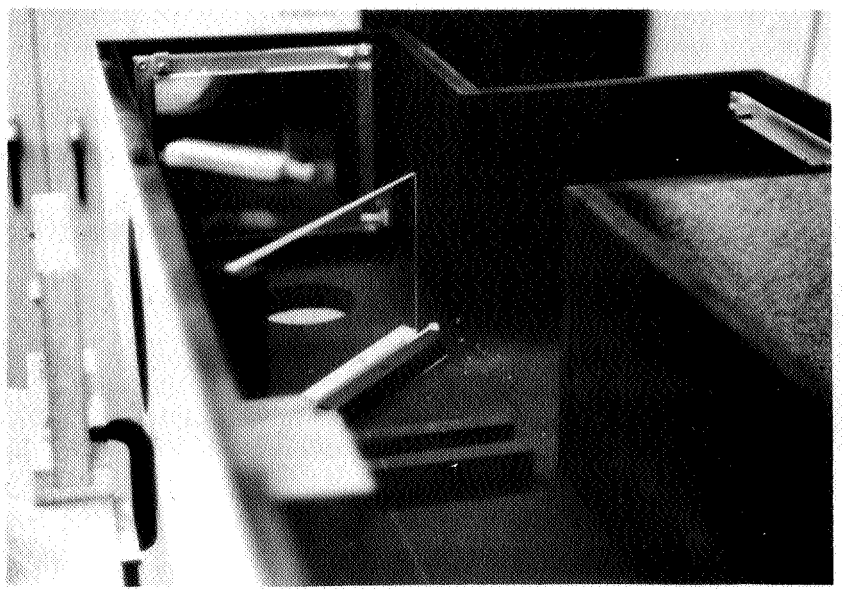

Fig. 10-2. Photograph of the Michelson holographic interferometer used with the pulsed ruby laser. The beam splitter and two end mirrors are shown. The laser beam is collimated and enters from the left. The spatial filter lens L_3 has been removed for the photograph.

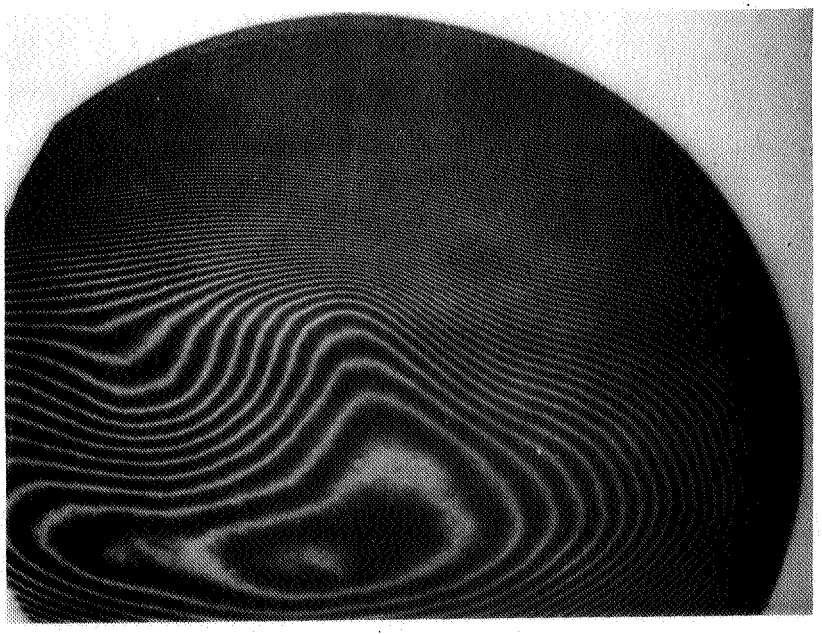

Fig. 10-3. A conventional 0° angle (non-holographic) interferogram showing the quality of the components of the Michelson system. The thin wedge beam splitter is responsible for most of the systems aberrations.

reflectivity (50% reflectivity is preferred, but the wedge used was one on hand for other purposes). Fig. 10-3 shows the fringe pattern resulting when the system was aligned for the least number of fringes (zero angle). Approximately 100 fringes are visible, indicating a system of very low optical quality if used for conventional interferometry.

The great number of residual fringes is several times too large to test the high order interferometric technique, because the aberrations are too great to permit separation of the high orders.

With a 1° angle between the scene and reference beam, one obtains on the hologram a fringe spacing of about 40 microns, sufficiently coarse to permit the use of high speed photographic materials. Because it was available, Kodak type IV-F spectrographic plates were used. To form holographic interferograms, two exposures are made on each plate. The comparison exposure is made first with the scene empty before firing the projectile. The second exposure is made while the projectile is in the scene volume. The developed plate is reconstructed with a parallel beam, duplicating the reference beam, with the arrangement shown in Fig. 10-4. The apparent focus of the subject was computed to be about 12 inches in front of the camera, and the camera (or eye) was focused at this point.

Fig. 10-5a shows a photograph of the reconstruction of an infinite fringe interferogram. Taken at atmospheric pressure, one obtains twice the number of fringes as are present in an interferogram produced by a single pass interferometer (see, e.g., Fig. 2-2). Fig. 10-5b shows a finite fringe interferogram of a similar event. To make the finite fringe interferogram, the angle of the reference mirror was changed slightly (10° turn of the adjustment screw) between exposures. In both cases, the laser emitted small pulses about a microsecond after the primary Q-switched pulse. Multiple pulsing is thought to be primarily responsible for the fine multiple fringes near the shock front. Another possible cause is diffraction effects caused from the two longitudinally separated images in the double pass interferometer. Elimination of the

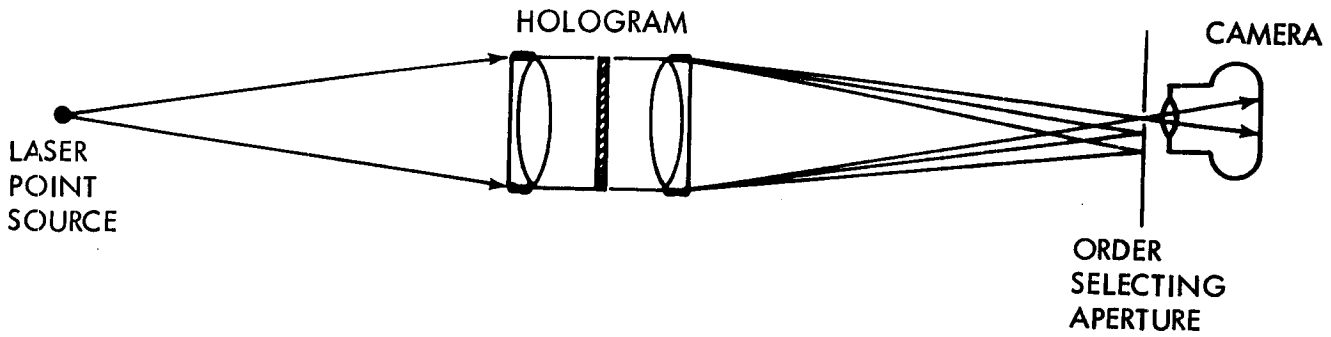

Fig. 10-4. Optical schematic of the arrangement used to reconstruct the holograms.

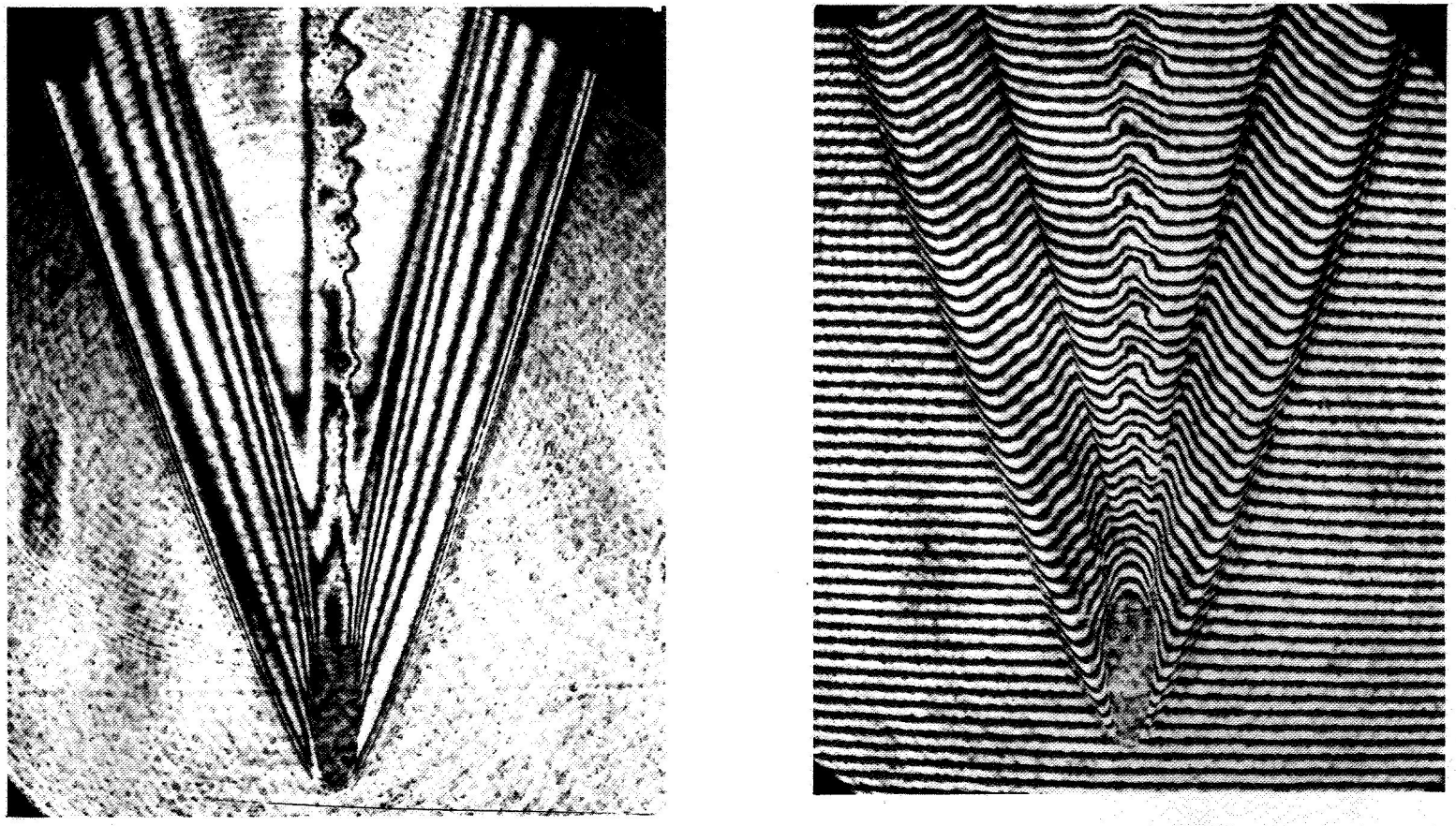

Fig. 10-5. (a) Infinite fringe holographic interferogram of a 22-250 bullet traveling in air at a velocity of approximately 3800 ft/sec. Multiple fringes visible near the nose of the projectile is believed to be due to small laser "after pulses."
(b) Finite fringe holographic interferogram of the same type event. The finite fringes are introduced by changing the angle of the reference beam slightly between exposures. The greater the angular change, the more closely spaced are the fringes. Very slight distortion in the finite fringes is believed to be due to a slight air turbulence or vibration and a slight "shearing" interferogram of the poor optics.

multiple pulses should resolve this question. The background noise in the photograph is due in great part to amplitude irregularities in the reconstructing beam.

The primary significance of these results is to demonstrate the ease with which interferograms can be made with poor optical components and a nonrigid structure. The laser coherence requirements are so minimal that any pulsed ruby laser should perform well in this system.

11.0 APPENDIX I

Derivation of the Relation Between Minimum Intensity of A Phase-Cancelled Interferogram and the Phase Sensitivity of the System

Consider the interference produced by two optical waves. Let the first have amplitude $1 + \eta$. Let the second have amplitude 1 and let it have a phase $\phi + 180°$ from the first wave. Then the sum of the two amplitudes can be represented by

$$(1+\eta) - e^{j\phi} ,$$

and the intensity of the resultant is given by

$$\begin{aligned} I &= \left((1 + \eta) - e^{j\phi}\right)\left((1 + \eta) - e^{-j\phi}\right) \\ &= 1 + (1 + \eta)^2 - 2(1 + \eta)\cos\phi \\ &= \eta^2 + 4(1 + \eta)\sin^2\frac{\phi}{2} \end{aligned}$$

If we denote by I_{min} the intensity when $\phi = 0$ and by I_{max} the intensity when $\phi = 180°$, we have

$$I = I_{min} + (I_{max} - I_{min})\sin^2\frac{\phi}{2} \quad . \tag{1}$$

From this we obtain

$$\frac{dI}{d\phi} = (I_{max} - I_{min})\frac{1}{2}\sin\phi \ .$$

Thus

$$\frac{\Delta I}{I} = \frac{(I_{max} - I_{min})\frac{1}{2}\sin\phi}{I_{min} + (I_{max} - I_{min})\sin^2\frac{\phi}{2}}\Delta\phi = C(\phi)\,\Delta\phi \ . \tag{2}$$

The value of ϕ which maximizes $C(\phi)$, maximizes the small perturbation phase sensitivity of $\frac{\Delta I}{I}$. Solving $\frac{dC(\phi)}{d\phi} = 0$ gives

$$\phi = \cos^{-1}\left(\frac{I_{max} - I_{min}}{I_{max} + I_{min}}\right).$$

which maximizes the phase sensitivity.

For the case where $I_{min} << I_{max}$, the case of present interest, the power series expansion gives

$$\phi \simeq 2\sqrt{\frac{I_{min}}{I_{max}}}$$

Thus setting the phase to this value, rather than 180° which corresponds to $\phi = 0$, optimizes the phase sensitivity of the interferogram for small phase perturbations.

For this optimum ϕ, formula (2) reduces to

$$\Delta\phi = 2\sqrt{\frac{I_{min}}{I_{max}}}\ \frac{\Delta I}{I}, \qquad (3)$$

where again higher order terms in I_{min}/ I_{max} have been ignored. This formula gives the scaling of the small perturbation phase sensitivity as a function of the ratio of the minimum to maximum intensity. In particular, it shows that to gain an order of magnitude in phase sensitivity requires two orders of magnitude reduction of I_{min}.

In view of the form of formula (1), it appears that the derivation of the formulas following (1) would apply even in the case where I_{min} is set by factors other than inequality of the intensities of the two beams. That is, it appears that the formula (3) is applicable also to cases where I_{min} is due primarily to scattering in the emulsion or to other extraneous sources which prevent complete cancellation.

12.0 APPENDIX II

Derivation of Formulas for the Location of Finite Fringes

Fig. 12-1 shows the geometry described in Section 6. When the diffusing surface is given a rigid rotation about the point C, of a small angle δ, the extra optical path introduced, for the rays from the scattering point P, is shown by the heavy line segments AP' and BP' of Fig. 12-1. In the limit of small δ, the arc PP' becomes the hypotenuse of right triangles PBP' and PAP'. The hypotenuse has length $\rho\delta$. The side AP' then has length $\rho\delta \sin\psi$ and the side BP' has length $\rho\delta\sin\beta$. Thus the length of the excess path introduced by the rotation is

$$E = \rho\delta(\sin\psi + \sin\beta) \quad . \tag{4}$$

Now this excess path E depends upon where the point P is located on the surface, for the parameters ρ, β, and ψ depend on the particular location of P on the surface. More specifically, if we introduce a variable point Q on the surface, defined by the angle μ as shown in Fig. 12-2, the path excess E_Q will be a function of μ. What we need to know in order to determine the location and spacing of the fringes is the rate of change of E_Q with respect to μ at $\mu = 0$.

A page or so of geometric calculation will yield the following value for $\frac{dE_Q}{d\mu}$ at $\mu = 0$:

$$\left.\frac{dE_Q}{d\mu}\right|_{\mu=0} = -\frac{\delta r}{\sin\gamma}\left\{\sin\gamma + \sin\theta - \frac{\rho}{r}\sin\gamma\cos\beta - \frac{\rho}{R}\cos\psi\sin\theta\right\} \tag{5}$$

Now we may make use of this formula in two different ways. In the first application we ask what value of r will make $\left.\frac{dE_Q}{d\mu}\right|_{\mu=0} = 0$? The value of r satisfying this condition gives the location of the focus of the fringes, for then all rays through a lens with axis on the line VP and focused on this

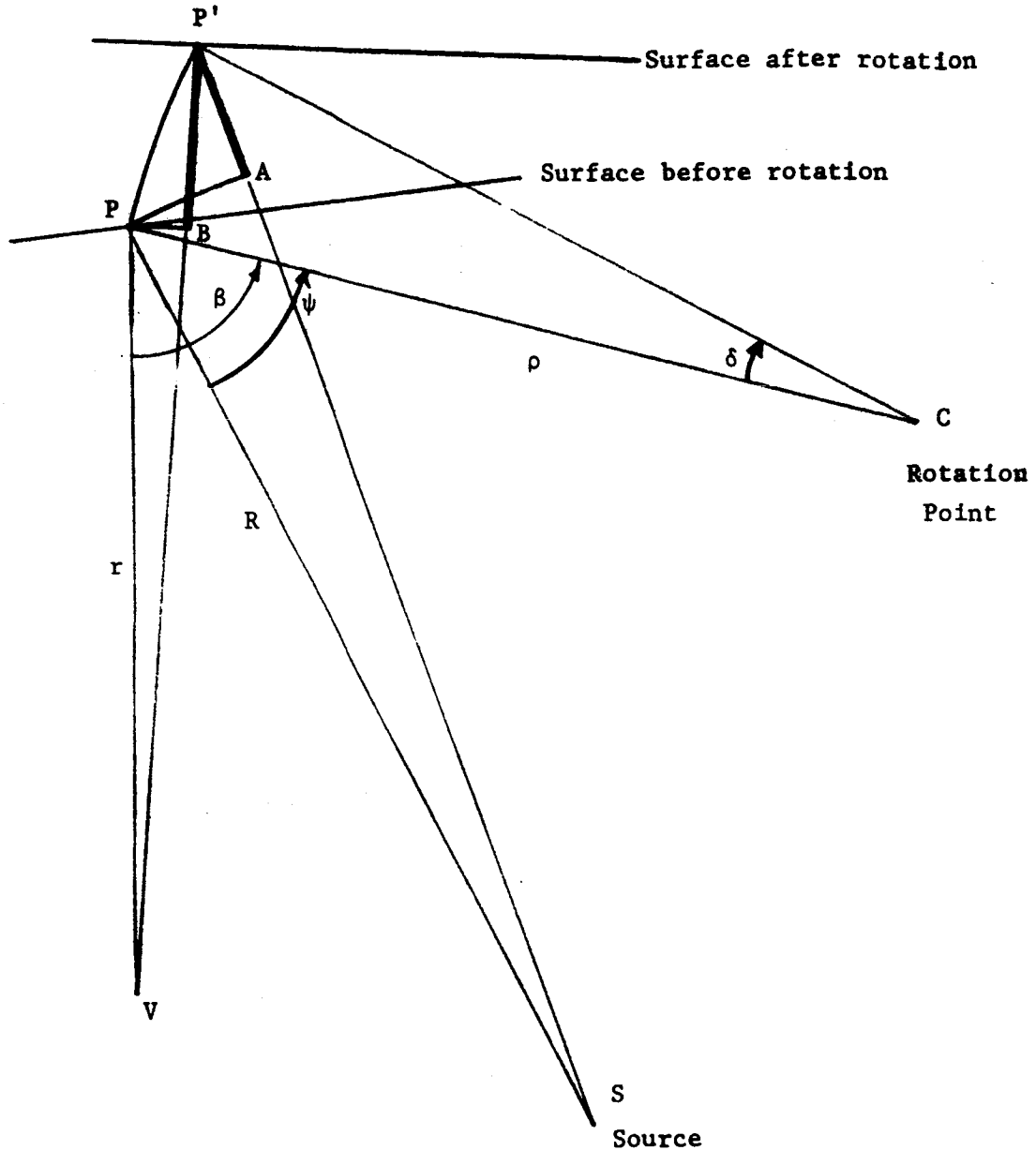
P'
Surface after rotation
A
Surface before rotation
P
B
β
ψ
ρ
δ
C
Rotation
Point
R
r
V
S
Source

Figure 12-1

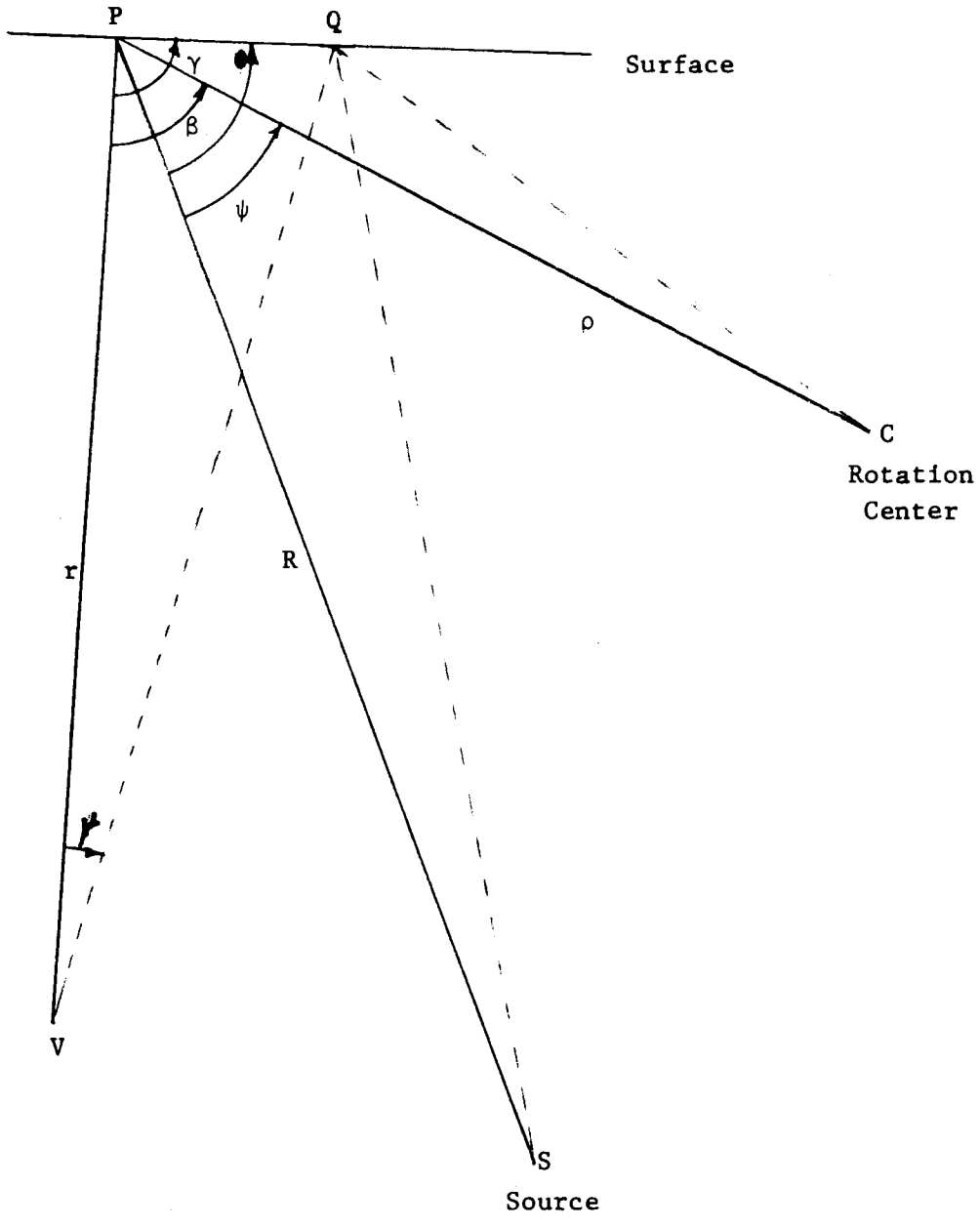

Figure 12-2

location on the line VP will have suffered the same amount of path excess. From (5), the value of r which satisfies the above condition, denoted by r_f, is

$$r_f = (\rho\cos\beta)\,\frac{1}{1 + \frac{\sin\theta}{\sin\gamma}\left(1 - \frac{\rho\cos\psi}{R}\right)} \quad .$$

The second application is to let r_0 be the distance to the viewer's eye, and then to determine the angular spacing of the fringes as seen by him. The angular separation $\Delta\mu$ of adjacent fringes is given by the condition

$$\left.\frac{dE_Q}{d\mu}\right|_{\substack{\mu=0 \\ r=r_0}} \Delta\mu = \lambda \ ,$$

where λ is the wavelength of light. Note that in this case the derivative is evaluated at $r = r_0$. If the spacing as a length is desired, for example in the focal plane of the fringes, then one multiplies $\Delta\mu$ by the distance to the fringe focal plane, namely $r_0 - r_f$. When this is done with equation (5) and the above conditions, the fringe spacing S in the fringe focal plane is found to be

$$S = \frac{\lambda}{\delta}\left(1 - \frac{r_f}{r_0}\right)\frac{1}{1 + \frac{\sin\theta}{\sin\gamma}\left(1 - \frac{\rho\cos\psi}{R}\right) - \frac{\rho}{r_0}\cos\beta} \quad .$$

13.0 REFERENCES

1. R. E. Brooks, L. O. Heflinger, and R. F. Wuerker, "Pulsed Laser Holograms," IEEE Journal of Quantum Electronics, QU-2, 275 (1966).

2. L. O. Heflinger, R. F. Wuerker, and R. E. Brooks, "Holographic Interferometry," J. of Appl. Phys., 37 (2) 642, February 1966.

3. R. E. Brooks, L. O. Heflinger, and R. F. Wuerker, "Interferometry With a Holographically Reconstructed Comparison Beam," Appl. Phys. Lett. 7, 248 (1965).

4. R. E. Brooks, L.O. Heflinger, R. F. Wuerker, and R. A. Briones, "Holographic Photography of High Speed Phenomena With Conventional and Q-Switched Ruby Lasers," Appl. Phys. Lett. 7, 92 (1965).

5. R. E. Brooks, "Low-Angle Holographic Interferometry Using Tri-X Pan Film," Applied Optics, 6, 1418 (1967).